MAX-PLANCK-INSTITUT FÜR PLASMAPHYSIK

GARCHING BEI MÜNCHEN

Coupling and Absorption of Lower-Hybrid Waves in a Thermonuclear Plasma

S. Puri, M. Tutter

IPP IV/82 March 1975

Die nachstehende Arbeit wurde im Rahmen des Vertrages zwischen dem Max-Planck-Institut für Plasmaphysik und der Europäischen Atomgemeinschaft über die Zusammenarbeit auf dem Gebiete der Plasmaphysik durchgeführt.

IPP IV/82 S. Puri
M. Tutter

Coupling and Absorption of Lower-Hybrid Waves in a Thermonuclear Plasma

March 1975 (in English)

ABSTRACT

The three important aspects, namely (i) accessibility, (ii) matching and (iii) absorption of the lower-hybrid waves in a thermonuclear plasma are studied under idealized but physically pertinent conditions within the framework of linearized theory. After two successive linear mode conversions--from an electromagnetic to a plasma wave and from the plasma to an electrostatic wave, respectively--the energy of the wave is deposited into the plasma ions in the presence of magnetic field gradients. The first of these mode conversions occurs when the radially inward directed electromagnetic wave (known as the slow or the shear cold-plasma wave) encounters a critical density which is somewhat below the lower-hybrid density. It is found that the propagation of the electromagnetic wave as well as the location of the mode conversion is unaffected by the presence of cyclotron-harmonic resonances on the path of the wave. The advance of the radially outward

---

* Based on the review paper presented at the "Second International Congress on Waves and Instabilities in Plasmas", Innsbruck, March 1975

propagating plasma wave, on the contrary, is readily checked by a cyclotron harmonic, thereby preventing the wave from transporting the rf energy back to the plasma edge. This results in the second wave conversion and the resultant electrostatic wave is readily absorbed on an encounter with an ion-cyclotron-harmonic resonance. It is shown that linear wave conversion is a very general phenomenon occuring at every confluence of real and complex waves in a lossless inhomogeneous medium. Computed values of the plasma surface impedance for a wide range of the longitudinal refractive index are presented to facilitate the design of both slow-wave and grazing-incidence coupling schemes for several existing or projected machines (WEGA, ATC, W VII, ASDEX, FT, PLT and the PPPL REACTOR). It is proposed that the difficult problem of frequency tracking necessary to heat the flat-topped thermonuclear plasmas near their core might be circumvented by the deliberate choice of a frequency well below the maximum lower-hybrid frequency in the plasma. In this scheme the rf energy introduced at the top (or bottom) access of the torus is carried to the plasma middle after both the wave conversions have already taken place near the edge of the plasma. It appears that the Buchsbaum's two-ion hybrid resonance might be the ideal method of heating thermonuclear reactor plasmas.

1. INTRODUCTION

The dispersion relation obtained by Aström [1] for waves in a multi-species, cold, collisionless, homogeneous, magnetized plasma may be expressed in the form

$$n_x^2 = \frac{\epsilon_{xx}\tilde{\epsilon}_{xx} - \epsilon_{xy}^2 + \tilde{\epsilon}_{xx}\epsilon_{zz}}{2\epsilon_{xx}} \pm \left[\left(\frac{\epsilon_{xx}\tilde{\epsilon}_{xx} - \epsilon_{xy}^2 + \tilde{\epsilon}_{xx}\epsilon_{zz}}{2\epsilon_{xx}}\right)^2 + \frac{\epsilon_{zz}}{\epsilon_{xx}}\left(\epsilon_{xx}^2 - \tilde{\epsilon}_{xx}^2\right)\right]^{1/2} \qquad (1)$$

where

$$\epsilon_{xx} = 1 - \sum_j \frac{\Pi^2}{1-\Omega^2}\,, \qquad (2)$$

$$\epsilon_{xy} = -i \sum_j \frac{\Pi^2\Omega}{1-\Omega^2}\,, \qquad (3)$$

$$\epsilon_{zz} = 1 - \sum_j \Pi^2\,, \qquad (4)$$

are the elements of the dielectric tensor

$$\underline{\underline{\epsilon}} = \begin{pmatrix} \epsilon_{xx} & \epsilon_{xy} & 0 \\ -\epsilon_{xy} & \epsilon_{xx} & 0 \\ 0 & 0 & \epsilon_{zz} \end{pmatrix}, \qquad (5)$$

$\Pi = \omega_p/\omega$, $\Omega = \omega_c/\omega$, $n_x = ck_x/\omega$, $n_z = ck_z/\omega$, j

denotes the particle type (suffix j will be dropped unless an ambiguity exists), s_j is the sign of the charge carried by the particle, and $\tilde{\epsilon}_{xx} = \epsilon_{xx} - \nu_z^2$. The right-hand coordinate system is oriented such that the plane of propagation lies in the x-z plane with the static magnetic field B_o aligned along the z-direction. Unless otherwise stated, rationalized MKS system of units is employed throughout the paper. All field quantities are assumed to possess a space and time dependence exp i $(k_x x + k_z z - \omega t)$ with no variation along the y-direction. Resistivity correction $\Delta\underline{\underline{\epsilon}}$ to the dielectric tensor is incorporated by using the method given by Stix [2] ,

$$\Delta\underline{\underline{\epsilon}} = i(\omega \nu_{ei}/\omega_{pe}^2)\ (\underline{\underline{\epsilon}} - \underline{\underline{I}})\cdot(\underline{\underline{\epsilon}} - \underline{\underline{I}}), \qquad (6)$$

where ν_{ei} is the electron-ion collision frequency and $\underline{\underline{I}}$ is the identity tensor. Corresponding to the four roots of (1), the x-components of the electric fields associated with the four waves in the plasma are

$$E_{x\pm}^{f,s} = \hat{E}_{x\pm}^{f,s} \exp i\left(k_{x\pm}^{f,s} x + k_z z - \omega t\right) \qquad (7)$$

while the remaining field components E_y, E_z, H_x, H_y, and H_z may be derived from the Maxwell's equations,

$$\underline{k} \times \underline{E} = \omega \underline{B} \qquad (8)$$

$$\underline{k} \times \underline{H} = -\omega \underline{D} \tag{9}$$

$$\underline{k} \cdot \underline{D} = 0 \tag{10}$$

$$\underline{k} \cdot \underline{B} = 0 \tag{11}$$

$$\underline{D} = \epsilon_0 \underline{\underline{\epsilon}} \cdot \underline{E} = \epsilon_0 \underline{E} + \underline{P} \tag{12}$$

$$\underline{B} = \mu_0 \underline{\underline{\mu}} \cdot \underline{H} = \mu_0 (\underline{H} + \underline{M}) \tag{13}$$

and

$$\underline{J} = -i\omega \underline{P} + i \underline{k} \times \underline{M} \tag{14}$$

where $\underline{J}$ is the total plasma current, $\underline{P}$ the polarization vector and $\underline{M}$ the magnetization vector. Note that we have employed the symmetric formulation of the Maxwell's equations in terms of $\underline{E}$, $\underline{H}$, $\underline{D}$ and $\underline{B}$. The components of $\underline{\underline{\mu}}$ may be expressed in a form identical to that of $\underline{\underline{\epsilon}}$ in (5). For the cold-plasma case, $\underline{\underline{\mu}} = \underline{\underline{I}}$.

The symmetric formulation possesses the advantage that the tangential components of $\underline{E}$ and $\underline{H}$ are continuous even when $\underline{\underline{\mu}}$ differs from the identity tensor which is a useful property for solving boundary value problems in stratified media [3]. In (8) the indices f and s correspond, respectively, to the smaller and the larger roots of ν_x^2. The first of these will be referred to as the fast (electromagnetic), oblique-compressional or the quasi-ordinary mode. The second root is the slow

(electromagnetic), oblique-shear, quasi-extraordinary, or simply the hybrid wave which encounters the resonance at the hybrid resonances as $\epsilon_{xx} \to 0$. For a three-component plasma (electrons, deuterium and tritium) this occurs when

$$1 - \frac{\Pi_e^2}{1-\Omega_e^2} - \frac{\Pi_D^2}{1-\Omega_D^2} - \frac{\Pi_T^2}{1-\Omega_T^2} = 0 \qquad (15)$$

For high frequencies, the last two terms on the left are negligibly small, so that

$$\omega^2 = \omega_{pe}^2 + \omega_{ce}^2 = \omega_{uh}^2 \qquad (16)$$

is a solution of (15). This is the upper-hybrid resonance and has been known since the early ionospheric research. As ω is lowered in (15), then for some $\omega_{cD} < \omega < \omega_{ce}$, either the second or the third term in (15) can be made to dominate, and ϵ_{xx} assumes respectively large positive or negative values. Evidently ϵ_{xx} vanishes for some intermediate frequency. This is the lower-hybrid resonance frequency approximately given by

$$\omega^2 \simeq \omega_{pD}^2 + \omega_{pT}^2 + \omega_{cD}\,\omega_{cT} \simeq \omega_{lh}^2 \,. \qquad (17)$$

Some of the earliest references to the lower-hybrid resonance occur in the works of Körper [4] and Auer et al [5]. Using similar arguments it follows that

further lowering of ω results in one more root of (15) in the frequency range $\omega_{cT} < \omega < \omega_{cD}$. This is the ion-ion hybrid resonance of Buchsbaum [6] occuring at

$$\omega \approx \left(\omega_{cD}\, \omega_{cT}\right)^{1/2} \simeq \omega_{ih} \qquad (18)$$

If a plane wave of amplitude E_y^o in vacuum is incident normally on a magnetized plasma slab of uniform density, then since $k_x^p \cdot D_x^p = k_x^p \cdot (\epsilon_{xx} E_x^p + \epsilon_{xy} E_y^p) = 0$, it follows that in the plasma

$$E_x^p = -(\epsilon_{xy}/\epsilon_{xx})\, E_y^p \,. \qquad (19)$$

Near the plasma edge $E_y^p = E_y^o$ so that $E_x^p \to \infty$ as $\epsilon_{xx} \to 0$ and the energy density at the plasma edge $\mathcal{E} \simeq (1/2)\, \epsilon_o\, \epsilon_{xx}\, (E_x^p)^2 = (1/2)\, \epsilon_o\, \epsilon_{xy}^2\, (E_y^o)^2/\epsilon_{xx}$ diverges leading to a strong surface heating.

Since plasmas of practical interest are not homogeneous, surface heating is readily avoided by a proper choice of ω so that the hybrid resonance occurs deep inside the plasma column. The success of such a scheme depends upon the ability of the rf energy to traverse the low-density region between the plasma edge and the resonant density. This would be the case if ν_x is real everywhere between the antenna and the resonant layer. From an analysis of (1), Stix [2] concluded that the propagation condition is satisfied (except in a narrow region of inconsequential importance near the

plasma edge) if

$$\nu_z^2 > \nu_{zc}^2 = 2\left(1 + \omega_{pe}^{*2}/\omega_{ce}^2\right), \quad (20)$$

where the asterik denotes the value at the location of the resonance. A somewhat less demanding sufficiency condition for accessibility, namely

$$\nu_z^2 > \nu_{zc}^2 = 1 + \left(\omega_{pe}^*/\omega_{ce}\right)^2 \quad (21a)$$

was subsequently derived by Parker [7] and Golant [8]. Another useful form of (21a) may be expressed as

$$\nu_z^2 > \nu_{zc}^2 = 1 + 2\left(\frac{m}{M_D}\right)N^2 \quad (21b)$$

for an equal deuterium-tritium mixture; m and M_D are the electron and deuterium masses, and $N = \omega/\omega_{cD}$ is the approximate cyclotron harmonic for ω. Several variants and refinements of (20) may be found in Refs. [9-11]. Waves with $\nu_z > 1$ are referred to as slow or retarded waves. Due to heavy demands on the label "slow" elsewhere in this paper, we shall adopt the terminology "retarded" waves when $\nu_z > 1$. Consequently we shall call the waves with $\nu_z < 1$ as "unretarded" waves.

Another important contribution made by Parker [7] and Golant [8] is the recognition that it is the transverse-magnetic (TM) vacuum wave which dominantly couples to the slow electromagnetic (or the lower-

hybrid) wave. For the practical realization of a retarded TM wave antenna, Golant [8] suggested the use of a Millman line (Fig. 1) while Parker [7] recommended a mechanically less cumbersome method using a waveguide flush-mounted on the machine wall. More sophisticated variants of Parker's scheme called a "phased array" or a "grill" have been proposed by Karney, Bers and Kulp [12] and by Lallia [13]. These consist of an array of waveguides flush-mounted on the torus wall with phasing appropriate for producing the required retardation (Fig. 2). By concentrating the ν_z spectrum in a relatively narrow accessible region this system could, in principle, provide superior coupling between the plasma and the rf source.

An antenna may be regarded as an intermediary between the plasma and the rf generator. An ideal antenna must simultaneously fulfil the twin requirements of wave "accessibility" into the plasma as well as of presenting a "matched load" impedance into the generator. Furthermore it must be "mechanically simple". Of the coupling configurations hitherto described, the Millman line promises good accessibility and matching, whereas the "phased array" has the advantages of mechanical simplicity and accessibility.

In yet another approach (Fig. 3), known as the "grazing-incidence" coupling [14], optimum matching and mechanical simplicity are stressed. For this case, $\nu_z \simeq 1$ and the accessibility condition (21) is not

fulfilled. The price exacted for simplicity in matching is that there is a region of evanescence near the plasma boundary. If $(\omega^*_{pe}/\omega_{ce})^2 \ll 1$ or for low values of N, the evanescent region is thin enough to allow tunneling of the rf energy [15, 16]. This method is suitable for coupling to relatively low-density plasmas.

The rf wave launched from an antenna situated in vacuum gradually converts into a slow electrostatic wave as it advances into the inhomogeneous plasma of ever-increasing density. Within the cold-plasma approximation, the wave is collisionally absorbed [2, 17] as it encounters the lower-hybrid resonance. At higher temperatures, however, the collisional absorption becomes ineffective [18]. Stix [18, 19] pointed out that instead of absorption, the radially inward propagating slow electromagnetic wave undergoes "linear mode conversion" into a radially outward propagating warm "plasma wave". This important result has been subsequently confirmed by several authors [9, 20-27]. Possibility of a second wave conversion of the "plasma" wave into a radially inward propagating "electrostatic" Gross-Bernstein [28-30] wave at low plasma densities near the plasma edge has been recently conjectured by Simonutti [31] and proved by Wong and Tang [32].

In this paper it will be shown that the inclusion of magnetic field gradients adds subtle and interesting effects with respect to the second wave conversion and the collisionless absorption processes. Extensive

computed results for the plasma surface impedance of several representative low-ß torus machines are presented to facilitate the design of antenna structures. Difficulties and possible remedies for various coupling schemes are outlined, whenever possible, in quantitative terms. Since the coupling schemes are dependent on the absorption mechanisms, their treatment is deferred till Secs. III and IV, while the problems of wave absorption in a hot plasma are taken up in Sec. II.

2. LOWER-HYBRID DISPERSION CHARACTERISTICS IN A HOT PLASMA

In thermonuclear plasmas of practical interest either the scale length of the density gradient or the local value of wavelength is well in excess of the ion-Larmor radius. In either case, the "local" hot-plasma dielectric tensor description would yield acceptably accurate results. Anticipating the boundary conditions to be used in future computations, we shall employ the Derfler-Omura [33] dielectric and diamagnetic tensors given by

$$\epsilon_{xx} = 1 + \sum_j \frac{\pi^2}{\Omega} \rho_0 e^{-\lambda} \sum_{-\infty}^{\infty} \frac{n}{\lambda} I_n(\lambda) Z_n , \qquad (22)$$

$$\epsilon_{xy} = -i \sum_j s_j \frac{\pi^2}{\Omega} \rho_0 e^{-\lambda} \sum_{-\infty}^{\infty} \left[I_n(\lambda) - I_n'(\lambda) \right] Z_n , \qquad (23)$$

$$\epsilon_{zz} = 1 - \sum_j \pi^2 \rho_0^2 e^{-\lambda} \sum_{-\infty}^{\infty} I_n(\lambda) Z_n' , \qquad (24)$$

and

$$\underline{\underline{\mu}} = \left(\underline{\underline{I}} - \underline{\underline{\chi}} \right)^{-1} , \qquad (25)$$

where

$$\chi_{xx} = \sum_j \frac{\pi^2}{2 \Omega \nu_z^2} e^{-\lambda} \sum_{-\infty}^{\infty} \frac{n}{\lambda} I_n(\lambda) Z_n' , \qquad (26)$$

$$\chi_{xy} = -i \sum_j s_j \frac{\pi^2}{2\Omega\nu_z^2} e^{-\lambda} \sum_{-\infty}^{\infty} \left[I_n(\lambda) - I_n'(\lambda) \right] Z_n' , \quad (27)$$

$$\chi_{zz} = \sum_j \frac{\pi^2 V^2}{\Omega^2 \nu_z} e^{-\lambda} \sum_{-\infty}^{\infty} \left[I_n(\lambda) - I_n'(\lambda) Z_n , \right. \quad (28)$$

$$\zeta_n = \frac{1 - n\Omega}{\nu_z V} , \quad (29)$$

$$\lambda = \frac{\nu_x^2 V^2}{2\Omega^2} , \quad (30)$$

$Z_n' = dZ_n/d\zeta_n$, $V = v/c$, v is the particle thermal velocity $I_n(\lambda)$ is the modified Bessel function in the notation of Watson [34] , $Z_n = Z(\zeta_n)$ is the Fried's function [35] defined as

$$Z(\zeta_n) = \pi^{-1/2} \int_{-\infty}^{\infty} \frac{e^{-x^2}}{x - \zeta_n} dx , \quad Im(\zeta_n) > 0 , \quad (31)$$

$I_n'(\lambda) = dI_n(\lambda)/d\lambda$ and $Z_n' = dZ_n/d\zeta_n$. Since in the derivation of the Derfler-Omura tensor, the total plasma current is subdivided into the polarization and magnetization currents, the tangential magnetic field at a boundary is continuous. In every other respect, this tensor is identical to the forms derived by Stepanov [36] and Stix [2] . Although the original derivation of the Derfler-Omura [33] dielectric tensor follows

directly from the Boltzmann's equation, an alternative method of obtaining it from the Stepanov [36] tensor is outlined in Appendix A [37].

Eliminating $\underline{E}$ and $\underline{H}$ in (8)-(13) gives the dispersion relation in the form

$$a\,\nu_x^4 + b\,\nu_x^2 + c = 0\,, \tag{32}$$

where

$$a = \epsilon_{xx}\,\mu_{xx}\,, \tag{33}$$

$$b = \nu_z^2\,(\epsilon_{xx}\mu_{zz} + \epsilon_{zz}\mu_{xx}) - \epsilon_{xx}\,\epsilon_{zz}\,(\mu_{xx}^2 + \mu_{xy}^2) - \mu_{xx}\,\mu_{zz}\,(\epsilon_{xx}^2 + \epsilon_{xy}^2)\,, \tag{34}$$

$$c = \epsilon_{zz}\,\mu_{zz}\,[\nu_z^4 + 2\nu_z^2\,(\epsilon_{xy}\mu_{xy} - \epsilon_{xx}\mu_{xx}) + (\epsilon_{xx}^2 + \epsilon_{xy}^2)(\mu_{xx}^2 + \mu_{xy}^2)]\,. \tag{35}$$

In this section we shall limit our attention to a two-component plasma in which the electrons and ions (deuterium) possess isotropic maxwellian velocity distributions of equal temperature. Equation [32] possesses an infinite number of solutions, most of which are complex. Several useful properties of these solutions follow from broadly general considerations without explicitly solving the equation:

(i) For real ω and k_z, the imaginary part of k_x may never cross the zero axis for arbitrary parameter variations, because the addition of an infinitesimal loss requires that $I_m(k_x) \neq 0$.

(ii) If the rf sources are situated at $x \leq 0$ then for $x > 0$ only waves with $I_m(k_x) > 0$ may exist in an infinite, homogeneous plasma. Furthermore, the energy flow, and hence the group velocity $v_{gx} = \partial\omega / \partial k_x$, must be directed along the positive x-direction. It follows that waves with $Re(k_x) > 0$ correspond to forward waves while the backward waves are characterized by a negative value of $Re(k_x)$. In other words, the forward or backward character of the wave at any point in the parameter space can be uniquely determined from a knowledge of k_x at that point.

(iii) For the case of no loss (or negligibly small loss) an inspection of (32) shows that complex values of λ or k_x occur in conjugate pairs. It then follows from (ii) above that backward and forward waves must exist in pairs in the vicinity of points in the parameter space where propagation changes into evanescence. Such points are commonly referred to as "confluence" points. The preceding arguments imply that all confluence points involve one backward and one forward propagating wave turning into a conjugate pair of evanescent waves. In Appendix B it is shown that a backward wave approaching a confluence point from the propagation side will convert into a forward wave receding from the confluence

point in the propagation side and vice versa .

(iv) Even in a fully lossless hot plasma, the tensors $\underline{\underline{\epsilon}}$ and $\underline{\underline{\mu}}$ are non-hermitian in the region of complex waves, i.e., losslessness does not necessarily imply hermiticity. Conversely, a non-hermitian dielectric tensor is necessary but not a sufficient criterion for the existence of dissipative absorption. For complex, lossless waves, non-hermiticity of $\underline{\underline{\epsilon}}$ and $\underline{\underline{\mu}}$ merely implies that the wave energy is being redistributed between the Poynting and the kinematic fluxes.

Of the two cold-plasma modes, the slow electromagnetic mode is profoundly affected by the inclusion of the hot-plasma effects, whereas the fast electromagnetic mode takes scant notice of any temperature changes. This can be seen from Fig. 4 where k_x is plotted as a function of plasma density for several values of the temperature for both the fast and the slow modes [38]. The dielectric tensor component ϵ_{xx} which plays an important role in the lower-hybrid wave is shown in Fig. 5. The longitudinal refractive index $\nu_z = 0.99$ for all these curves which have been obtained through an exact (accuracy exceeding one part in a million) numerical solution of (32). For low temperatures, both the fast and the slow modes exhibit propagation on the low-density side of the lower-hybrid resonance except near the plasma edge where complex

waves are seen to exist because the value of $\nu_z < 1$ chosen does not satisfy the accessibility condition (21). On the high-density side of the resonance (shown by a cross on the density axis), the fast mode continues to propagate while the slow mode becomes evanescent. Introduction of electron resistivity modifies this behaviour somewhat and the resultant cold-plasma waves are absorbed through collisions at the hybrid layer. For the parameters chosen, collisionless ion-cyclotron harmonic damping is quite negligible.

Observe that the slow mode is a backward wave (recognized by the opposite signs of the real and the imaginary parts of k_x) which for lower temperatures transforms into a forward wave upon passing through the cutoff on the high density side of the resonance. The fast electromagnetic wave, on the other hand, remains a forward wave throughout. A confluence of this pair of backward and forward waves occurs near $n_p \simeq 1 \times 10^{13}$ cm^{-3}. Yet another confluence takes place very near the plasma edge for $n_p \sim (m/M) n_p^*$.

For increasing temperatures, collisional absorption decreases and for $T \gtrsim 10$ eV ceases to play any significant role [18]. For still higher temperatures the ion-Larmor radius becomes comparable with the wavelength of the slow mode. This has the effect of inhibiting the magnitude of k_x. Also the evanescence

occurs somewhat in advance of the hybrid layer, resulting in significantly altered appearance of the dispersion characteristics for $T \gtrsim 1$ keV. At these high temperatures ϵ_{xx} becomes complex in the evanescent region so that $\underline{\underline{\epsilon}}$ is non-hermitian. This does not, however, imply energy dissipation [39] for reasons already mentioned.

Existence of complex waves under almost lossless conditions does, on the other hand, demand the existence of a complex conjugate solution with a propagating counterpart beyond the confluence point. This is the so-called "plasma" wave which joins smoothly to the lower-hybrid wave at the confluence point as shown in Fig. 6. Since the slow electromagnetic wave is a backward wave, it follows that the plasma wave must be a forward wave. The energy of the lower-hybrid wave upon reaching the confluence point completely converts into the plasma wave and starts to propagate towards the plasma edge. This important mechanism known as "linear wave conversion" was discovered by Stix [19] who used singular-turning-point techniques to solve the fourth-order differential equation in the vicinity of $\epsilon_{xx} = 0$. Although ϵ_{xx} never vanishes for a hot plasma, the results obtained by Stix remain valid in the light of the arguments presented in Appendix B.

The plasma wave travelling towards the plasma edge, in its own turn, becomes evanescent for low densities.

Evidently the existence of yet another wave, this time a backward one, is necessary. This is the so-called "electrostatic" wave (Fig. 6) studied, among others, by Gross [28], Bernstein [29], and Fredricks [30]. The joining together of the "slow" wave, the "plasma" wave, and the "electrostatic" wave is depicted in a qualitative manner by Stix [19], while quantitative plots for the warm-plasma approximation are given in Pešić [24]. The possibility of a second wave conversion from the plasma wave to the electrostatic wave has been conjectured by Simonutti [31] and proved by Wong and Tang [32] in a derivation containing significant modifications of the techniques used by Stix [19]. The complete dispersion curve of Fig. 6 has been computed without any simplifying assumptions.

Collisionless wave absorption occurs when the particles feel the electric field in phase for an extended duration. This occurs when ζ_n in (29) is in the neighbourhood of unity. It will be shown later that coupling considerations dictate that $\nu_z \lesssim 2$ for efficient energy transfer from the antenna to the plasma. Also $(c/v_i) \sim 10^2\text{-}10^3$ so that collisionless absorption is possible only in an extremely narrow vicinity of the cyclotron-harmonic frequencies. In a practical situation using a uniform magnetic field, it would be difficult to maintain the field to such a close tolerance. Consequently, in a typical situation the electro-

static wave will propagate right across the plasma column where, after an inverse series of wave conversions successively into plasma and slow electromagnetic waves, the rf energy will eventually escape into vacuum as shown in Fig. 7. This signals the necessity of having magnetic field gradients for the absorption of the lower-hybrid wave.

3. EFFECT OF MAGNETIC FIELD GRADIENTS

In an actual thermonuclear device like a torus, the wave of frequency ω launched near the plasma edge is obliged to traverse through several harmonics of the ion-cyclotron frequency before it arrives at the hybrid layer. A radical modification in the wave behaviour in the vicinity of the cyclotron harmonics cannot be apriori ruled out. In case the cyclotron harmonics are not transparent to the wave, the rf energy will be deposited close to the plasma edge and the entire concept of accessibility to the plasma core will have to be revised. This, fortunately, is not the case [38] as may be seen from the dispersion characteristics (Fig. 8) obtained in the presence of magnetic field gradients. The dispersion characteristics for both the fast and the slow waves are scarcely affected and completely ignore the presence of the seven (9th-15th, shown by circles on the density axis) cyclotron harmonics on their path.

The reason for the above behaviour may be understood by noting that for the values of λ (in the neighbourhood of unity) for the lower-hybrid wave $I_n(\lambda)$ becomes extremely small for $9 \leqslant n \leqslant 15$ thereby precluding the possibility of a large contribution to the summations (22)-(28) by the Fried's function Z_n in the vicinity of the harmonics.

The effect of the magnetic field gradient in the computations of Fig. 8 has been simulated by a fictitious d-c current in the y-direction such that B_o decreases [40] linearly with increasing density from the value $B_o = 150$ kG at the plasma edge to $B_o = 100$ kG at the hybrid layer. As before, "local" dielectric tensor approximation is employed under the stipulation that either the wavelength or the scale length of the gradient sufficiently exceeds the ion-Larmor radius.

Subsequent behaviour of the lower-hybrid wave is dependent on the magnetic field gradient and the following four cases arise.

3.1. Coupling from the Outer Circumference of Torus

The radially inward propagating slow electromagnetic wave encounters positive density as well as magnetic field gradients (Fig. 9a). At a density somewhat below the lower-hybrid density, it converts into a radially outgoing "plasma" wave. Unlike the lower-hybrid wave, the plasma wave is sensitive to the magnetic field variations

and is unable to pierce through the cyclotron harmonic. Instead it converts into the electrostatic mode which propagates radially inwards until it encounters the next cyclotron harmonic, where it is absorbed through the collisionless damping processes (Fig. 9b), the wave energy going into the perpendicular ion motion. Observe that the magnetic field gradients effectively trap the radio frequency energy between the adjacent harmonics which enclose the region of the first wave conversion [41].

3.2. Coupling from the Inner Circumference of Torus

In this case the radially inwards advancing wave front encounters a positive density gradient but a negative magnetic field gradient. The lower-hybrid wave then smoothly joins the plasma wave [41] which in turn converts into the electrostatic wave (Fig. 10) as it approaches a cyclotron harmonic. The electrostatic wave is eventually absorbed, as before, on an encounter with the cyclotron-harmonic resonance (Fig. 9b).

The typical thermonuclear requirements for the ignition of low-β plasmas using supplementary heating is to raise the temperature of the ohmically heated plasmas from approximately 1 to 10 keV. An examination of Fig. 4 reveals that the density at the first wave conversion region reduces by about 20% as the plasma temperature changes from 1 to 10 keV. For the steep density profiles predicted in thermonuclear plasmas

[42], the wave conversion, and consequently the heating, might move uncomfortably close to the plasma edge as the temperature of the plasma increases. Density profiles for several values of p are shown in Fig. 11; p = 1 corresponds to linear profile, p = 2 to a parabolic variations, etc.

An even more difficult problem must be faced in the selection of the rf frequency itself. For a steep density profile an exceedingly accurate control of the plasma density, as well as the profile shape, will have to be exercised to insure heating near the plasma core, since it will not be possible to change the frequency after an investment of several tens of millions of dollars towards the purchase of the rf equipment.

3.3. Coupling from the Top or Bottom of the Plasma Column

One method of overcoming both the difficulties mentioned above would be to inject the rf energy from the top or bottom of the plasma column deliberately at a frequency somewhat lower than the lower-hybrid frequency at the center of the plasma column. Due to the steep density profile both the wave conversions occur close to the plasma edge. After the second wave conversion, the radially inward propagating electrostatic wave tends to bend in the direction of the magnetic field gradient in an attempt to orient itself along $\nabla\nu$, orthogonal to the surfaces of constant refractive index (Fig. 21a). It is, as before, absorbed at the cyclotron-harmonic resonance.

Since the actual frequency used is no longer critical, the choice of frequency and the planning for the rf equipment required can be carried out in advance of the knowledge of the actual plasma parameters. A subsequent change in the plasma parameters, e.g., the center density, would not involve any alterations of the rf equipment.

If the adjacent harmonics are spaced sufficiently apart, the rf energy might be fairly evenly deposited along the plasma radius. The spacing between the harmonics can, or course, be increased simply by using a lower frequency, as shown in Fig. 12b.

3.4. Coupling to Very Low Cyclotron Harmonics

The process of lowering the frequency can be continued, in principle, till ω equals the ion-cyclotron frequency, below which the lower-hybrid resonance disappears. For $\omega_{ci} < \omega < 2\ \omega_{ci}$, it is possible to choose the frequency in such a manner that no cyclotron-harmonic (or cyclotron) resonance occurs between the outer plasma edge and the resonant region occurring near the major radius of the torus. Under such circumstances it is advantageous to revert back to launching the rf waves from an antenna situated at the outer torus circumference. Coupling from the inner edge is not possible because the incident wave travelling against the magnetic field gradient will be reflected rather than absorbed at the cyclotron harmonic.

An interesting semantic question comes up concerning the nomenclature "lower-hybrid heating" when referring to such low harmonics of the ion-cyclotron frequency. The label "ion-cyclotron heating", on the other hand, could be confused with the approach in which the compressional wave coupled into the plasma by a TE antenna is absorbed due to the presence of a finite left-hand component in the electric field polarization [43, 44]. Perhaps an appropriate description for the present method would be "shear wave ion-cyclotron harmonic heating".

4. MATCHING AND ACCESSIBILITY

Irrespective of the method of coupling, the pertinent quantity for evaluating antenna performance and design is the surface impedance of the plasma defined as $\sigma_s = -(E_z/H_y)$ for TM waves and $\sigma_s = E_y/H_z$ for TE waves. The most powerful technique for dealing with such problems is through the use of the WKB analysis which assumes that the wave propagates without reflection if the refractive index is a slowly varying function of position. Although valid in the intermediate region, the so-called adiabaticity condition is severely violated both at the vacuum-plasma interface and near the resonant layer in the interior of the plasma. Using singular-turning-point analysis, Budden [17] and Stix [2] have shown that the wave propagages from the intermediate region to the

hybrid layer in a cold plasma and is completely absorbed without reflection. This is also confirmed through computations described in Sec. 4.1. In a hot plasma, adiabaticity is violated near the region of absorption of the electrostatic wave at the cyclotron-harmonic resonance. The conditions prevailing are practically identical to those treated in [2] and [17] for the cold-plasma case and one may safely assume that no reflection of the rf energy occurs from the absorption region in spite of the breakdown of the WKB assumptions.

The crucial question of a possible mismatch at the vacuum-plasma interface has been treated by Parker [7] and Golant [8]. A pivotal assumption in their analysis requiring the absence of reflected waves beyond the low-density cutoff occurring near $\omega_{pe} = \omega$ is, however, not borne out by the exact computations to be described in Sec. 4.1. for even the largest plasmas of practical interest. An elegant improvement over the WKB approach has been recently introduced by Wong and Tang [32] who treat the boundary between propagation and evanescence as a confluence point which can then be treated using extensions of the familiar wave conversion techniques.

Previously we have described computational techniques capable of yielding almost exact results for the plasma surface impedance [14,15,45] for plasmas of small transverse dimensions. In this paper these results will

be extended to plasmas of arbitrarily large sizes. We shall take advantage of the fact that, except for a relatively narrow region near the plasma edge, the WKB requirements of complete transmission are justified. The width "t" of this region determined from numerical computations is in no case found to exceed 10 cm. The plasma surface impedance is, therefore, not materially affected if the plasma column beyond the depth t from the plasma edge is replaced by a plasma of uniform density existing at t. Since only a thin shell of a reactor plasma of several meters diameter determines the surface impedance, use of a slab instead of a toroidal geometry for the determination of σ_s will give reasonably accurate results. Two cases of interest using the retarded and unretarded waves, respectively, are treated in the following sections. Since the dispersion characteristics near the plasma boundary are unaffected by temperature effects (see Fig. 4), considerable simplification is gained by using the cold-plasma model

4.1. Coupling using Retarded Waves

The slab model used for determining the plasma surface impedance consists of a plasma half-space extending from $x = 0$ to $x = \infty$. The axes are oriented such that the static magnetic field B_o is along the

z-direction and the propagation vector $\underline{k}$ lies in the x-z plane (Fig. 13). The slow wave TM antenna situated at x = -b consists of a magnetic sheet current

$$J_s = J_o \exp i(k_z z - \omega t) \tag{36}$$

of amplitude $J_o = 1$ W s^{-1} cm^{-1} so that E_z has a discontinuity at x = -b. Such an antenna is an ideal representation of a Millman line. The plasma density is assumed to possess the form

$$\frac{n}{n_o} = \begin{cases} 1 - \left(\frac{g-x}{g}\right)^p & \text{for } x \leq g \\ 1 & \text{for } x > g \end{cases} \tag{37}$$

For reasons outlined earlier the density will be truncated at x = t well ahead of the hybrid layer without significantly affecting the outcome of the computations so far as the determination of σ_s is concerned. The actual value of t to be used is determined by trial. During the computations t is gradually increased till σ_s attains a stable value. It is found empirically that t equal to h/2 or 10 cm (whichever is smaller) is sufficient for the purpose. The density profile is taken into account using a stratified model. The region $0 < x < t$ is stratified into 99 slabs, while $x > t$ forms the 100th slab. The plasma density is assumed to be uniform in each slab. The model becomes exact as the number of slabs tends to infinity and the thickness of each slab tends to zero. In practice, an

acceptable approximation is obtained by making each plasma slab much thinner than the local value of the wavelength. There are four waves of amplitudes $E_{x\pm}^{f,s}$ in each plasma slab except in the slab to the right of $x > t$ which has only two waves, one fast and one slow, each of which decays for increasing x, there being no sources at infinity. In the vacuum region $-b < x < 0$ between the current sheet and the plasma boundary there are, in general, four waves, two TE and two TM, while in the region $x < -b$ to the left of the current sheet there are only two waves, one TE and one TM, both of which decay for decreasing x.

It can be readily verified that the number of undetermined quantities equals the boundary conditions requiring the continuity of the tangential components of the electric and magnetic fields. The resultant set of 400 complex, linear, algebraic equations is solved using standard computational routines. In order to maintain the maximum computational accuracy, the slab widths Δx are adjusted so that the phase change $\Delta\phi = \left|k_x^s \Delta x\right|$ in each slab is approximately equal. Typically $\Delta\phi/2\pi < 1/30$ in each of the slabs. A large concentration of slabs is introduced near the plasma edge in the vicintiy of the low-density cutoff where the departure from the WKB conditions is most pronounced. Checks performed on the continuity of the normal components of the Poynting vector $1/2\ (\underline{E} \times \underline{H}^*)_x$, electric displacement $\epsilon_o\ (\underline{\underline{K}} \cdot \underline{E})_x$ and magnetic induction $\mu_o H_x$ across each of

the slab boundaries indicated a computational accuracy exceeding one part in a million. Similar accuracy exists in a more stringent test establishing in each plasma slab the equality of the divergence of the Poynting vector, $\nabla \cdot \left[1/2\ (\underline{E} \times \underline{H}^*)\right]$ with the rate of change of stored energy, $-(i\omega/2)\left\{\epsilon_o\ (\underline{E}^* \cdot \underline{\underline{K}} \cdot \underline{E}) - \mu_o\ \underline{H} \cdot \underline{H}^*\right\}$.

For small $h \lesssim 5$ cm it was found that σ_s remains essentially unchanged as t is varied from $0.5h$ to $1.3h$ confirming the validity of the WKB assumption near the hybrid layer. On the other hand, increasing t beyond the low-density cutoff produces substantial changes in σ_s underlining the inadequacy of the WKB analysis in this region.

Figure 14 shows the computed values of surface impedance normalized with respect to the free space impedance $\sigma_s/\eta = -\left[E_z/H_y\right]_{x=0}$ for ν_z ranging between 1.2 and 5.0 for two different plasma profiles using the parameters of the Princeton conceptual reactor [46]. The real and the imaginary parts of σ_s/η are approximately equal and vary between 0.1 and 2.0 as ν_z increases from 1.2 to 5. Effect of a steeper profile either by an increase in p (Fig. 14) or by a decrease in g (Fig. 15) results in a reduction in the value of σ_s.

In a practical application the antenna is not located in direct contact with the plasma surface. As such, the quantity pertinent to antenna design is the surface impedance presented by the plasma at the

position $x = -b$ of the antenna. Figure 16 shows the variation in σ_s as a function of b. Whereas the reactive component of σ_s remains fairly constant, the resistive part changes by several orders of magnitude for changes in b of only a few centimeters except for the case $\nu_z = 1.2$. Therefore, in order to avoid serious matching problems in the presence of relatively minor displacements of the plasma column, the minimum value of ν_z consistent with the accessibility condition (21) must be used. The decrease in the surface resistance for increasing b is a straightforward consequence of the requirement that the x-component of the Poynting vector has to remain constant, while the electric field increases almost exponentially as the antenna is approached.

For ν_z of the order of 1.2, the normalized surface impedance presented by the plasma at the antenna is roughly 0.1. The normalized surface impedance of a rectangular waveguide operating in the fundamental TE_{10} mode is given by

$$\frac{\sigma_g}{\eta} = \left[1 - \left(\frac{\lambda}{2a_g}\right)^2\right]^{-1/2} \qquad (38)$$

where a_g is the larger of the two transverse dimensions of the waveguide. The minimum value of σ_g/η in (38) occurs for $a_g \to \infty$, when

$$\left[\sigma_g/\eta\right]_{min} = 1. \qquad (39)$$

Since the minimum waveguide surface impedance is about 10 times larger than the surface impedance presented by the plasma, one has to contend with reflection coefficients of the order of 0.9 when using a phased array for coupling the rf energy into the plasma. Exact matching and complete transmission, in principle, are still possible by using stub tuners (or other reactive devices like posts or irises) provided energy densities near the plasma surface over a hundred times larger than for the case of a perfect match can be tolerated. An important modification to these considerations will occur if a relatively tenuous plasma of density of the order of $(m/M)n_{lh}$ extends till the reactor walls so that b is effectively zero. It would then be advantageous to use larger value of ν_z offering more favourable matching possibilities.

The surface impedance computations of Figs. 14-16 assumed an antenna of infinite extension in the z-direction. In practice it suffices for the antenna to be long enough such that the bulk of the rf energy has been transferred from the antenna into the plasma. The absorption length, l_{abs}, defined as the distance over which $\left(1 - e^{-1}\right)$ or approximately 64% of the initial energy of the antenna has entered the plasma, depends on ν_z, b and the plasma surface impedance. Derivation of l_{abs}/λ_o is given in Appendix C while the computed values for the Princeton reactor are

shown in Fig. 17. The antenna length necessary to effectively transfer the rf energy into the plasma increases rapidly with b (or b/λ_o). This is not surprising because the retarded wave tends to "stick" to the antenna surface and the electric field at the plasma decays exponentially with b. As previously pointed out, it is always possible to match the "phased array" to the plasma using suitable reactive devices, irrespective of the length of the array. One must, however, pay the price with a reduction in the plasma surface impedance and an increase in the reflection coefficient and the voltage-standing-wave ratio (VSWR).

The real part of the surface impedance for several other machines listed in Table I are shown in Fig. 18 assuming a linear density profile. As already pointed out, somewhat smaller values of σ_s are to be expected for steeper profiles. The imaginary part of σ_s (not shown in the figure) is for all practical purposes equal to the real part. The general trand is towards a decreasing σ_s for the smaller machines. The resultant increase in the VSWR and the reflection coefficient may be acceptable due to the lower power levels involved. Other considerations similar to the ones discussed for the reactor are applicable.

4.2. Grazing Incidence Coupling

For ω corresponding to the low harmonics of the ion-cyclotron frequency, effective coupling to the hybrid-resonance is possible using grazing angle incidence with $\nu_z \simeq 1$. Once again plasma surface impedance completely specifies the antenna design. The geometry for determining σ_s is similar to the one used for the case of retarded waves except that instead of a current sheet excitation, the rf energy is carried by a unit amplitude TM wave, incident on the plasma surface at an angle φ as shown in Fig. 19. Part of the incident energy is transmitted into the plasma half-space, the remaining being reflected partly as a TM and partly as a TE wave with amplitudes R_{TM} and R_{TE}, respectively.

The normalized surface impedance for a linear plasma profile is shown as a function of φ (Fig. 20) for the parameters of the Princeton reactor for three different values of $N = (\omega/\omega_{cD})$. The resistive part of (σ_s/η) is of the order of 10^{-2} and as expected decreases steadily with increasing N. This tendency is also confirmed in Fig. 21, where the fractional transmitted power $1-R^2$, where $R^2 = R_{TM}^2 + R_{TE}^2$ is plotted as a function of φ. For the unretarded waves an improvement in accessibility is to be expected for steeper density profiles. There is also a small capacitive reactive component of the surface impedance shown magnified by a factor of 10 in Fig. 20.

To appreciate the significance of these results, let

us consider the boundary value problem of the grazing incidence coupling. The geometry of Fig. 3 may be idealized to admit of analytical tractability without loss of essential physics. The cylindrical geometry will be replaced by a slab model (Fig. 22) and variations in the y-direction will be ignored. We assume that only the dominant mode is present in the coupling waveguide. For the TM mode in the plasma waveguide

$$H = H_y = \hat{H}_y \cos(k_x x) \exp i(k_z z), \qquad (40)$$

where the time dependence has been dropped. From (40) and (9),

$$E_x = \hat{H}_y k_z/\omega\epsilon_o \cos(k_x x) \exp i(k_z z), \qquad (41)$$

and

$$E_z = -\hat{H}_y i k_x/\omega\epsilon_o \sin(k_x x) \exp i(k_z z), \qquad (42)$$

The form (40) for H_y was selected in anticipation of the boundary condition $E_z = 0$ at $x = 0$ in the plasma waveguide. The second boundary condition $-E_z/H_y = \sigma_s$ at $x = b$ yields the dispersion relation

$$\nu_x \tan(\nu_x 2\pi b/\lambda_o) = -i\sigma_s/\eta . \qquad (43)$$

Note that in this case b is the separation of the plasma boundary from the machine walls. Since $\sigma_s/\eta \ll 1$ for the unretarded waves (Fig. 20), one of the solutions of (43) is given by

$$\nu_x^2 = -i\left(\frac{\sigma_s}{\eta}\right)\frac{\lambda_o}{2\pi b} \quad . \tag{44}$$

Using $\sigma_s/\eta = 10^{-2}$, $\lambda_o/2\pi b = 1$, we obtain from the identity $\nu_x^2 + \nu_z^2 = 1$,

$$\nu_z \simeq 1 + i\,0.005 \tag{45}$$

which is in fact one of the modes found in our treatment of the plasma parallel-plate waveguide [47]. Since this mode resembles the TEM-like configuration of the coupling waveguide, almost all the incident energy will be coupled into this mode, i.e., impedance matching presents no problems in this approach. It is not necessary to know the exact value of φ corresponding to ν_z given in (45) because the plasma surface impedance is relatively insensitive to the precise value of φ in a sufficiently broad region.

From Appendix C the absorption length, l_{abs}, for this case is given by

$$l_{abs}/b = |\sigma_s/\eta|^{-1} \tag{46}$$

and is typically one hundred times the separation between the plasma and the torus wall. Requiring that l_{abs} may not exceed the torus circumference gives an upper bound on b of

$$b < 10^{-2}\, 2\pi A \qquad (47)$$

where A is the torus major radius. For the Princeton reactor this requires that the separation between the plasma and the inner wall should be kept below 60 cm.

There are undoubtedly further solutions of (43), as well as another class of normal modes of the plasma waveguide, with TE or mixed TM-TE character. Although very little rf energy is initially coupled to these modes, some is bound to be scattered from the TEM to these modes due to discontinuities invariably present. In case one of these modes happens to fulfil the accessibility condition and has a relatively high surface impedance, the TEM wave coupled through the grazing incidence could be absorbed over a shorter distance. Studies to explore such a possibility are presently in progress.

A pictorial appearance of grazing-incidence coupling to low ion-cyclotron harmonics in the Princeton reactor is depicted together with the transmission coefficient in fig. 23. In these computations the magnetic field gradients due to the finite aspect ratio have been included. Apparently $\omega = 2\,\omega_{cT}$ is the most convenient frequency requiring the smallest waveguide access. Similar computations have been carried out for several other representative machines and the recommendations for the grazing-incidence coupling for each of the machines are listed in

Table II. Note that, except for the three large machines, i.e., Princeton reactor, JET and PLT, waveguide coupling is not feasible and a TM coupling loop has to be used. Ironically this means a return to the problem of matching which we had sought to avoid in the first place using the grazing-incidence method!

5. DISCUSSION

The linearized treatment followed in this paper tacitly assumes that the energy density $\mathcal{E}_w$ in the rf wave is small compared to the thermal energy density. For the parameters of the Princeton reactor, if we assume that the rf energy is uniformly injected over the entire plasma surface and is responsible for supplying the entire heating in one second, the maximum of (for $T = 10^8$ °K)

$$\mathcal{E}_w / \mathcal{E}_{th} \sim O(10^{-5}) \qquad (48)$$

occurs near the region of the minimum group velocity which has been taken to be of the order of ion-thermal speed. In evaluating (48) an increase in $\mathcal{E}_w$ by a factor of ten has been included to account for the magnification in the energy density because of the cylindrical effects. A Further increase in $\mathcal{E}_w$ is to be foreseen because in practice the rf energy is coupled by an antenna of finite size rather than being introduced over the entire plasma surface. This enhancement in the field strength

is linked with the "resonance cone" effect of Kuehl [48]. Whether the field enhancement is sufficient to trigger parametric and non-linear effects can be decided only when accurate theories including the effects of plasma inhomogeneities become available. A review of the parametric instability theory is given in a recent paper by Porkolab [49].

Other possible absorption mechanisms not included in our treatment are due to stochastic [24,44] and magnetic field gradient effects [50]. The mechanism responsible for both these types of absorption is apparently Landau damping produced by an amnesia in the particle regarding its relative phase with respect to the electric field.

Returning to the question of coupling, some work is required to accurately estimate the extent of difficulties in the impedance matching of the "phased array". Also, since the phased array derives its property of wave retardation from mutual coupling and feedback among the array elements (waveguides), a stability analysis of this system with respect to perturbations in the plasma surface is needed.

The "grazing-incidence" coupling, as cited already has a rather long absorption length. Also due to the relatively low frequencies used, the lower-hybrid resonance and, consequently, the region of wave conversion lies close to the plasma edge. In the presence of cold

gas near the plasma edge, collisional effects would dissipate the wave leading to a wasteful heating of the plasma boundary.

One possible means of overcoming these objections would be by using Buchsbaum's two-ion-hybrid resonance in which case the resonance lies deep in the interior of the plasma and the wave conversions occur far from the edge. Since the problem of wave penetration is quite trivial, the grazing incidence method will simultaneously fulfil the matching and accessibility requirements at least for reactor size plasmas where waveguide coupling is still possible. In smaller plasmas where TM-loop coupling has to be employed, the problem of matching returns but perhaps in a form less serious than the other known techniques.

In a sense the increasing complexity of the theoretical analyses for answering the still outstanding problems becomes an exercise of ever-decreasing returns. The time is ripe for a vigorous experimental attack on lower-hybrid heating. The first laboratory experiments on lower-hybrid absorption were carried out by Schlüter [51] and later by the Austin group. The trajectory of the wave in a long non-uniform plasma and its eventual absorption at the hybrid layer was demonstrated by Briggs and Parker [52]. The verification of the cold-plasma dispersion has been done by Bellan and Porkolab [27] while resonance cones have been observed both by Bellan and Porkolab [27] and by Javel, Müller, and Weynants [53]. Parametric decay

has been observed by several authors cited in the review paper of Porkolab [49]. Actual demonstration of ion heating by lower-hybrid frequency has been made by Golant [54], Glagolev [55], as well as in the LIWEREX experiment currently in progress in Garching. Important new results should soon be forthcoming from the ALCATOR, ATC, and WEGA machines.

ACKNOWLEDGEMENTS

We are glad to acknowledge the help of Dr. H. Kuehl, Dr. F. Leuterer, Dr. M. Simonutti, Dr. T. H. Stix, and especially Dr. R. Weynants in dispelling some misconceptions held by the authors with regard to the behaviour of the lower-hybrid wave near the region of the first wave conversion. We are also thankful to Dr. K. C. Wong and Prof. T. Tang for pointing out the error in the sign of the reactive surface impedance of retarded waves in our previous work. We are indebted to Dr. F. Leuterer for the use of his derivation in Appendix A and to Dr. P. Barberio-Corsetti for providing us with the program [56] for computing the Fried's function.

This work was performed under the terms of the agreement on association between the Max-Planck-Institut für Plasmaphysik and EURATOM.

APPENDIX A

The symmetric formulation of the Maxwell's equations (8)-(14) is identical to the more familiar form

$$\underline{k} \times \underline{E} = \omega \underline{B} \tag{A1}$$

$$\underline{k} \times \frac{\underline{B}}{\mu_0} = -\omega \epsilon_0 \underline{\underline{K}} \cdot \underline{E} \tag{A2}$$

$$\nabla \cdot \epsilon_0 \underline{E} = \rho \tag{A3}$$

$$\nabla \cdot \underline{B} = 0 \tag{A4}$$

and

$$\underline{J} = -i\omega \epsilon_0 (\underline{\underline{K}} - \underline{\underline{I}}) \cdot \underline{E} \tag{A5}$$

in the sense that all macroscopic observables $\underline{E}$, $\underline{B}$ and $\underline{J}$ are the same. $\underline{\underline{K}}$ is the familiar form of the dielectric tensor [2,36]. From (8)-(14) and (25) we obtain

$$\underline{J} = -i\omega \epsilon_0 (\underline{\underline{\epsilon}} - \underline{\underline{I}}) \cdot \underline{E} + \frac{i}{\omega \mu_0} \underline{k} \times [\underline{\underline{\chi}} \cdot (\underline{k} \times \underline{E})] \tag{A6}$$

$$= -i\omega \epsilon_0 (\underline{\underline{\epsilon}} - \underline{\underline{I}}) \cdot \underline{E} + \frac{i}{\omega \mu_0} [\underline{k} \times (\underline{\underline{\chi}} \times \underline{k})] \cdot \underline{E}$$

Comparing (A5) and (A6) gives

$$\underline{\underline{K}} = \underline{\underline{\epsilon}} - \frac{c^2}{\omega^2} [\underline{k} \times (\underline{\underline{\chi}} \times \underline{k})] \tag{A7}$$

which finally gives $\underline{\underline{\epsilon}}$ and $\underline{\underline{\chi}}$ in terms of $\underline{\underline{K}}$

$$\chi_{xx} = - K_{xz} / (\nu_x \nu_z) , \tag{A8}$$

$$\chi_{xy} = K_{yz} / (\nu_x \nu_z) , \tag{A9}$$

$$\chi_{zz} = K_{yy} - K_{xx} , \tag{A10}$$

$$\epsilon_{xx} = K_{xx} + K_{xz} \nu_z / \nu_x , \tag{A11}$$

$$\epsilon_{xy} = K_{xy} - K_{yz} \nu_z / \nu_x , \tag{A12}$$

$$\epsilon_{zz} = K_{zz} + K_{xz} \nu_x / \nu_z . \tag{A13}$$

APPENDIX B

From (8)-(13) one obtains E_y, E_z, H_x, H_y and H_z in terms of E_x, defined as the wave amplitude,

$$E_y = (\Delta_1 / \Delta) E_x = \delta^1 E_x , \tag{B1}$$

$$E_z = (\Delta_2 / \Delta) E_x = \delta^2 E_x , \tag{B2}$$

$$H_x = (\Delta_3 / \Delta) E_x = \delta^3 E_x , \tag{B3}$$

$$H_y = (\Delta_4 / \Delta) E_x = \delta^4 E_x , \tag{B4}$$

and

$$H_z = (\Delta_5 / \Delta) E_x = \delta^5 E_x , \tag{B5}$$

where

$$\Delta = n_z \epsilon_{zz} (\epsilon_{xx} \mu_{xx} \mu_{zz} - \epsilon_{xy} \mu_{xy} \mu_{zz} - n_z^2 \mu_{zz} - n_x^2 \mu_{xx}) \quad (B6)$$

$$\Delta_1 = n_z \epsilon_{zz} \mu_{zz} (\epsilon_{xx} \mu_{xy} + \epsilon_{xy} \mu_{xx}) \quad (B7)$$

$$\Delta_2 = n_x (n_x^2 \epsilon_{xx} \mu_{xx} + n_z^2 \epsilon_{xx} \mu_{zz} - \epsilon_{xx}^2 \mu_{xx} \mu_{zz} - \epsilon_{xy}^2 \mu_{xy} \mu_{zz}) \quad (B8)$$

$$\Delta_3 = \epsilon_{zz} (n_x^2 \epsilon_{xx} \mu_{xy} - \epsilon_{xx}^2 \mu_{xy} \mu_{zz} - \epsilon_{xy}^2 \mu_{xy} \mu_{zz} - n_z^2 \epsilon_{xy} \mu_{zz}) \quad (B9)$$

$$\Delta_4 = \epsilon_{zz} (\epsilon_{xy}^2 \mu_{xx} \mu_{zz} + \epsilon_{xx}^2 \mu_{xx} \mu_{zz} - n_z^2 \epsilon_{xx} \mu_{zz} - n_x^2 \epsilon_{xx} \mu_{xx}) \quad (B10)$$

and

$$\Delta_5 = n_x n_z \epsilon_{zz} (\epsilon_{xy} \mu_{xx} + \epsilon_{xx} \mu_{xy}) \quad (B11)$$

Let x = 0 be the boundary (Fig. 24) separating the lossless regions, 1 and 2, such that a propagating forward wave and a propagating backward wave can exist in region 1, while a pair of evanescent complex conjugate waves are to be found in region 2. Consider a forward wave of amplitude F_{1i} originating at x = - ∞ incident

on the interface at x = 0. Part of the wave energy will be reflected as a forward wave of amplitude F_{1r}. Another part of the wave energy will be reflected as the backward wave of amplitude B_{1r}. Since the backward wave, too, has to transport the energy away from the boundary, its corresponding wave vector must be directed towards the interface. The rest of the incident energy is transmitted into region 2 as a forward wave (Re k > 0) of amplitude F_{2t} and a backward wave of amplitude B_{2t}. The four unknown quantities F_{1r}, B_{1r}, F_{2t}, and B_{2t} can be uniquely determined from the four boundary conditions requiring the continuity of the tangential components of E_y, E_z, H_y, and H_z at x = 0,

$$\delta_{1F}^{1}\left(F_{1i}+F_{1r}\right)+\delta_{1B}^{1}B_{1r}=\delta_{2}^{1}F_{2t}+\delta_{2}^{1*}B_{2t} \quad \text{(B12)}$$

$$\delta_{1F}^{2}\left(F_{1i}-F_{1r}\right)+\delta_{1B}^{2}B_{1r}=\delta_{2}^{2}F_{2t}-\delta_{2}^{2*}B_{2t} \quad \text{(B13)}$$

$$\delta_{1F}^{4}\left(F_{1i}+F_{1r}\right)+\delta_{1B}^{4}B_{1r}=\delta_{2}^{4}F_{2t}-\delta_{2}^{4*}B_{2t} \quad \text{(B14)}$$

$$\delta_{1F}^{5}\left(F_{1i}-F_{1r}\right)+\delta_{1B}^{5}B_{1r}=\delta_{2}^{5}F_{2t}-\delta_{2}^{5*}B_{2t} \quad \text{(B15)}$$

where on the RHS we have used the property that the δ's for the complex conjugate k's are also complex conjugate. This can be seen by inspection of (B6) till (B11) together with (22)-(30). Solving (B12) to (B15) for B_{1r} we obtain

$$B_{1r} / F_{1i} = -\xi \qquad \text{(B16)}$$

where

$$\xi = \frac{\begin{bmatrix} -\delta_{1F}^{1} & \delta_{1F}^{1} & \delta_{2}^{1} & \delta_{2}^{1*} \\ \delta_{1F}^{2} & \delta_{1F}^{2} & \delta_{2}^{2} & \delta_{2}^{2*} \\ -\delta_{1F}^{4} & \delta_{1F}^{4} & \delta_{2}^{4} & \delta_{2}^{4*} \\ \delta_{1F}^{5} & \delta_{1F}^{5} & \delta_{2}^{5} & \delta_{2}^{5*} \end{bmatrix}}{\begin{bmatrix} -\delta_{1F}^{1} & \delta_{1B}^{1} & \delta_{2}^{1} & \delta_{2}^{1*} \\ \delta_{1F}^{2} & \delta_{1B}^{2} & \delta_{2}^{2} & \delta_{2}^{2*} \\ -\delta_{1F}^{4} & \delta_{1B}^{4} & \delta_{2}^{4} & \delta_{2}^{4*} \\ \delta_{1F}^{5} & \delta_{1B}^{5} & \delta_{2}^{5} & \delta_{2}^{5*} \end{bmatrix}} \qquad \text{(B17)}$$

Similar expressions may be obtained also for F_{1r}, F_{2t}, and B_{2t}. Observe that

$$\xi \to 1, \quad \text{as} \quad \delta_{1F}^{i} \to \delta_{1B}^{i}, \quad i = 1 \text{ to } 5, \qquad \text{(B18)}$$

which is precisely the case near a confluence point. Also, as $(\delta_{1F}^{i} - \delta_{1B}^{i}) \to 0$, it can be shown that $F_{1r} \to 0$, i.e.,

all the energy in the forward wave has converted into the backward wave. Similarly, starting with a backward wave, it can be shown that the incident energy will be transferred into a reflected forward wave at the confluence point.

This proof can be extended to inhomogeneous plasmas using the stratified model described in Sec. 3. Since in a hot plasma $\underline{\underline{\epsilon}}$ and $\underline{k}$ are slowly varying functions of position including the confluence point itself, we may safely conclude from the above arguments that complete wave conversion from a forward to a backward wave, and vice versa, will transpire at every confluence of the propagating and evanescent regions.

A confluence point, however, does not have to be a region of wave conversion. If an oscillator was buried in region 2 of Fig. 24, it would simultaneously excite both the forward and the backward waves in region 1 propagating away from the boundary. Such a situation exists, in practice, near the plasma edge during the excitation of the fast and slow waves by an antenna placed in vacuum.

APPENDIX C

The absorption length, defined as the distance over which the power flowing in the vacuum region between the plasma and the coupling structure (Figs. 1,2, 22) reduces to e^{-1}, is given by

$$l_{abs} = \frac{1}{P_x} \int_0^b P_z(x)\, dx \qquad (C1)$$

where P_x and P_z are the components of the Poynting vector in vacuum along x and z directions, respectively. From (40)-(43) for the TM coupling

$$\frac{l_{abs}}{\lambda_o} = \frac{1}{8\pi} \frac{\nu_z}{\nu_x} \frac{1}{\sigma_{sr}} \left[\sin(2k_x b)\left(1 - \frac{|\sigma_s^2|}{\nu_x^2}\right) \right. \qquad (C2)$$

$$\left. - \frac{2\sigma_{si}}{\nu_x}\left(\cos 2k_x b - 1\right) + 2k_x b\left(1 + \frac{|\sigma_s^2|}{\nu_x^2}\right) \right]$$

which gives the absorption length normalized with respect to the vacuum wavelength in free space. The real and imaginary part of the plasma surface impedance σ_s are denoted by σ_{sr} and σ_{si}, respectively.

REFERENCES

1. ASTROM, E., Arkiv Fysik (1950) 443.
2. STIX, T. H., Theory of Plasma Waves, McGraw Hill, New York (1962).
3. DERFLER, H., private communication.
4. KORPER, von K., Z. Naturforsch. 12a (1957) 815.
5. AUER, P. L., HURWITZ, H. Jr., Miller, R. D., Phys. Fluids 1 (1958) 501.
6. BUCHSBAUM, S. J., Phys. Fluids 3 (1960) 418.
7. PARKER, R., QPR No. 102, Res. Lab. of Electronics, MIT, Cambridge, Mass. 97 (1971). In Parker's version of (20), the term $(\omega_{pe}/\omega_{ce})$ is not squared.
8. GOLANT, V. E., Zh. Tekh. Fiz. 41 (1971) 2492; Sov. Phys. Tech. Phys. 16 (1972) 1980.
9. GLAGOLEV, V. M., Plasma Physics 14 (1972) 301.
10. PEŠIĆ, S.S., Phys. Letters 38A (1972) 283.
11. ARTICO, G., SPIGLER, R., Plasma Physics 16 (1974) 1104.
12. KARNEY, C.F.F., BERS, A., KULP, J. L. APS Bulletin 18 (1973) Paper 2B15.
13. LALLIA, P., Symposium on Plasma Heating in Toroidal Devices, Varenna (1974) 120.
14. PURI, S., TUTTER, M., Z. Naturforsch. 28a (1973) 438.
15. PURI, S., TUTTER, M., Z. Naturforsch. 28a (1973) 1432.
16. PEŠIĆ, S.S., Second International Congress on Waves and Instabilities in Plasmas, Innsbruck (1975) Paper H5.
17. BUDDEN, K. G., Proc. Roy. Soc. A227 (1955) 516.
18. STIX, T. H., Phys. Fluids 3 (1960) 19.
19. STIX, T. H., Phys. Rev. Letters 15 (1965) 878.

20. KUEHL, H. H., Phys. Rev. 154 (1967) 124.

21. GORMAN, D., Phys. Fluids 9 (1966) 1262.

22. PILIYA, A. D., FEDOROV, V. I., Zh. Eksp. Teor. Fiz. 57 (1969) 1198; Sov. Phys. JETP 30 (1970) 653.

23. MOORE, B. N., OAKES, M. E., Phys. Fluids 15 (1972) 144.

24. PEŠIĆ, S. S., Plasma Physics 15 (1973) 193.

25. SIMONUTTI, M., Ph.D. dissertation, Massachusetts Institute of Technology (1974).

26. FIDONE, I., PARIS, R. B., Phys. Fluids 17 (1974) 1921.

27. BELLAN, P. M., PORKOLAB, M., Phys. Fluids 17 (1974) 1592.

28. GROSS, E. P., Phys. Rev. 82 (1951) 232.

29. BERNSTEIN, I. B., Phys. Rev. 109 (1958) 10.

30. FREDRICKS, R. W., J. Plasma Phys. 2 (1968) 365.

31. SIMONUTTI, M., private communication.

32. WONG, K. C., TANG, T., Second International Conference on Waves and Instabilities in Plasmas, Innsbruck (1975) Paper H7.

33. OMURA, M., Electrostatic Waves in Bounded Hot Plasmas, Stanford University IPP Rep. 156 (1967).

34. WATSON, G. N., Theory of Bessel Functions, Cambridge University Press (1922).

35. FRIED, B. D., CONTE, S. D., The Plasma Dispersion Function, Academic Press (1961).

36. STEPANOV, K. N., Sov. Phys. JETP 7 (1958) 892.

37. LEUTERER, F., private communication.

38. PURI, S., TUTTER, M., Finite Temperature Effects on the Lower-Hybrid Dispersion Characteristics, Max-Planck Institut für Plasmaphysik, Garching, Report IV/74 (1974).

39. An incorrect association of non-hermiticity of $\underline{\underline{\epsilon}}$ with dissipation is responsible for the wrong conclusions in the paper presented by the authors in the 1974 Varenna Conference on Plasma Heating in Toroidal Devices.

40.. Reversing the sign of ∇B_o does not affect the present conclusions.

41. Some exceptions to this picture will be discussed in a future communication dealing with computed ion-cyclotron harmonic dispersion curves. The results of this paper, however, remain substantially unchanged.

42. DUCHS, D., private communication.

43. ADAM, J., SAMAIN, A., EUR-CEA Report 579, Fontnay-aux-Roses (1971).

44. STIX, T. H., Symposium on Plasma Heating in Toroidal Devices, Varenna (1974) 105.

45. PURI, S., TUTTER, M., Nuclear Fusion 14 (1974) 93; The imaginary part of σ_s for TM waves is incorrect due to an error in the program. It was pointed out to us by Dr. T. Tang and Dr. K. C. Wong that the reactive component of σ_s should not be capacitive but inductive for this case.

46. RIBE, F. L., Fusion Reactor Systems , Los Alamos Scientific Labs. Report LA-UR 74-758.

47. PURI, S., TUTTER, M., Nuclear Fusion 13 (1973) 55.

48. KUEHL, H. H., Phys. Fluids 5 (1962) 1095.

49. PORKOLAB, M., Symposium on Plasma Heating in Toroidal Devices, Varenna (1974) 28.

50. BERS, A., private communication.

51. SCHLÜTER, H., Z. Naturforsch. 15a (1960) 281.

52. BRIGGS, R. J., PARKER, R. R., Phys. Rev. Letters 29 (1972) 852.

53. JAVEL, P., Müller , G. , Weynants, R., Second International Congress on Waves and Instabilities, Innsbruck (1975).

54. GOLANT, V. E., 5th Conference on Plasma Physics and Controlled Nuclear Fusion, Tokyo (1974).

55. GLAGOLEV, V. M., 5th Conference on Plasma Physics and Controlled Nuclear Fusion, Tokyo (1974).

56. BARBERIO-CORSETTI, Calculations of Plasma Dispersion Function, Princeton University Rep. Matt-773 (1970).

TABLE CAPTIONS

Table I Parameters of several representative low-β tori.

Table II Possible frequency and coupling geometry using grazing incidence.

FIGURE CAPTIONS

Fig. 1 Millman line coupling to the lower-hybrid resonance.

Fig. 2 Phased array or the "grill".

Fig. 3 Grazing-incidence coupling.

Fig. 4 Real (solid curve) and imaginary (dotted lines) parts of k_x versus density for both the fast and the slow waves as a function of temperature. The pair of curves for the slow mode are readily recognized by the resonance characteristics near the lower-hybrid density (shown by a cross on the density axis). The dashed lines in (d-f) correspond to the location of the reciprocal ion-Larmor radius ($|k_x r_{ci}| = 1$). For all these curves $\nu_z = 0.99$, $\omega / \omega_{cD} = 13.25$ and $B_o = 100$ kG. The vertical scale is compressed quadratically to facilitate the representation near the axis.

Fig. 5 Real (solid lines) and imaginary (dashed lines) parts of ϵ_{xx} vs. density for the parameters of Fig. 4. For higher temperatures ϵ_{xx} no longer vanishes at the hybrid layer shown by a cross on the density axis. The imaginary part of ϵ_{xx} arises from collisional dissipation at low temperatures ($T \lesssim 1$ eV). For higher temperatures ($T \gtrsim 10$ eV), on the other hand, the

imaginary part of ϵ_{xx} is due to evanescent waves notwithstanding the fact that $\underline{\underline{\epsilon}}$ is no longer hermitian.

Fig. 6 Composite dispersion characteristics of the fast (electromagnetic), the slow (electromagnetic), the plasma, and the electrostatic waves for T = 1 keV, $\nu_z = 0.99$, $B_o = 100$ kG, and $\omega / \omega_{cD} = 13.25$. The real and the imaginary parts are shown by the solid and the dashed curves, respectively.

Fig. 7 In the absence of magnetic field gradients, the lower-hybrid wave moves through the plasma column with four successive wave conversions but practically no dissipation.

Fig. 8 Effect of magneitc field gradient (B_o is 150 kG at the plasma edge and 100 kG at the hybrid layer) on the dispersion curves of Fig. 4 for case T = 10 eV. Ion-cyclotron harmonic numbers 9 to 15 are shown by circles on the density axis axis. For these curves, too, $\nu_z = 0.99$ and $\omega / \omega^*_{cD} = 13.25$.

Fig. 9 (a) Modification in the ion-cyclotron harmonic dispersion curves for ν_z finite and of the order of unity in the presence of density and magnetic field gradients. These qualitative curves are drawn for the case of the antenna located near the outer torus circumference, so that both the density and the magnetic field increase as the wave advances into the plasma center. The path of the wave is shown in (b).

Fig. 10 Same as Fig. 9 except that the wave encounters a negative magnetic field gradient if launched from the inner edge of the torus circumference.

Fig. 11 Shape of the plasma profile for several value of p defined in (37).

Fig. 12 Qualitative appearance of the ray path if the rf energy is introduced into the plasma from the top or bottom accesses of the torus. The general appearance changes from (a) to (b) as the frequency is lowered.

Fig. 13 Geometry used for computing the plasma surface impedance for retarded waves.

Fig. 14 σ_s/η versus ν_z for two different values of p for the Princeton reactor parameters.

Fig. 15 Effect of reducing g from 3 m to 3 cm leads to a reduction in σ_s by roughly one order of magnitude.

Fig. 16 Variation in σ_s with b, the separation between the antenna and the plasma surface.

Fig. 17 Absorption length determining the minimum antenna dimensions along the torus circumference for which the computed surface impedance values of this paper are applicable.

Fig. 18 Re(σ_s) versus ν_z for the parameters of the machines listed in Table I.

Fig. 19 Geometry for determining the plasma surface impedance for unretarded waves.

Fig. 20 σ_s versus φ for three different values of $N = \omega/\omega_{cD}$. The parameters of the Princeton conceptual reactors were used for the computations.

Fig. 21 Power transmitted into the plasma as a function of φ for the parameters of the Princeton reactor.

Fig. 22 Idealized geometry for grazing-incidence coupling.

Fig. 23 Grazing incidence to the low cyclotron harmonics in the Princeton reactor. The effect of the magnetic field gradients is included in the computations of the transmission coefficient. The insets are drawn approximately to scale.

Fig. 24 Reflection of a forward propagating wave into a propagating backward wave from a region of confluence between the propagating and evanescent waves. The propagation vector of the reflected backward wave in region 1 is directed opposite to the direction of the energy propagation indicated by the arrow.

Table I

	n_o cm^{-3}	gas	B_o kG	a cm	f_{lh} MHz	λ_o cm	v_{zc}
PRINC. REACTOR	1×10^{14}	D T	60	325	1200	25	1.13
JET	5×10^{13}	D	30	hor - 130 ver - 200	800	37	1.24
PLT	1×10^{14}	D	45	45	1200	25	1.18
FT	1×10^{14}	D	100	15	1400	22	1.05
ASDEX	3×10^{13}	H	30	40	950	32	1.15
W VII a,b	3×10^{13}	H	40	14(25)	1000	30	1.08
ATC	2×10^{13}	H	20	17	750	40	1.23
WEGA	3×10^{13}	H	15	15	700	42	1.50

Table II

	COUPLING	ACCESS	HARMONIC USED	f MHz	λ_o cm
PRINC. REACTOR	WAVEGUIDE	TOP*	$5\omega_{CD}$	229	130
	WAVEGUIDE	SIDE	$2\omega_{CT}$	91	330
JET	WAVEGUIDE	TOP	$13\omega_{CD}$	300	100
	TM LOOP	SIDE	$\omega_{CD}, 2\omega_{CD}$	22,45	
PLT	WAVEGUIDE	TOP	$15\omega_{CD}$	572	58
	TM LOOP	SIDE	$\omega_{CD}, 2\omega_{CD}$	38,76	
FT	WAVEGUIDE+	TOP	$15\omega_{CD}$	1140	27
	TM LOOP	SIDE	$\omega_{CD}, 2\omega_{CD}$	76,152	
ASDEX	TM LOOP	SIDE	$\omega_{CH}, 2\omega_{CH}$	46,92	
W VII	TM LOOP	SIDE	$\omega_{CH}, 2\omega_{CH}$	61,122	
ATC	TM LOOP	SIDE	$\omega_{CH}, 2\omega_{CH}$	30,61	
WEGA	TM LOOP	SIDE	$\omega_{CH}, 2\omega_{CH}$	23,46	

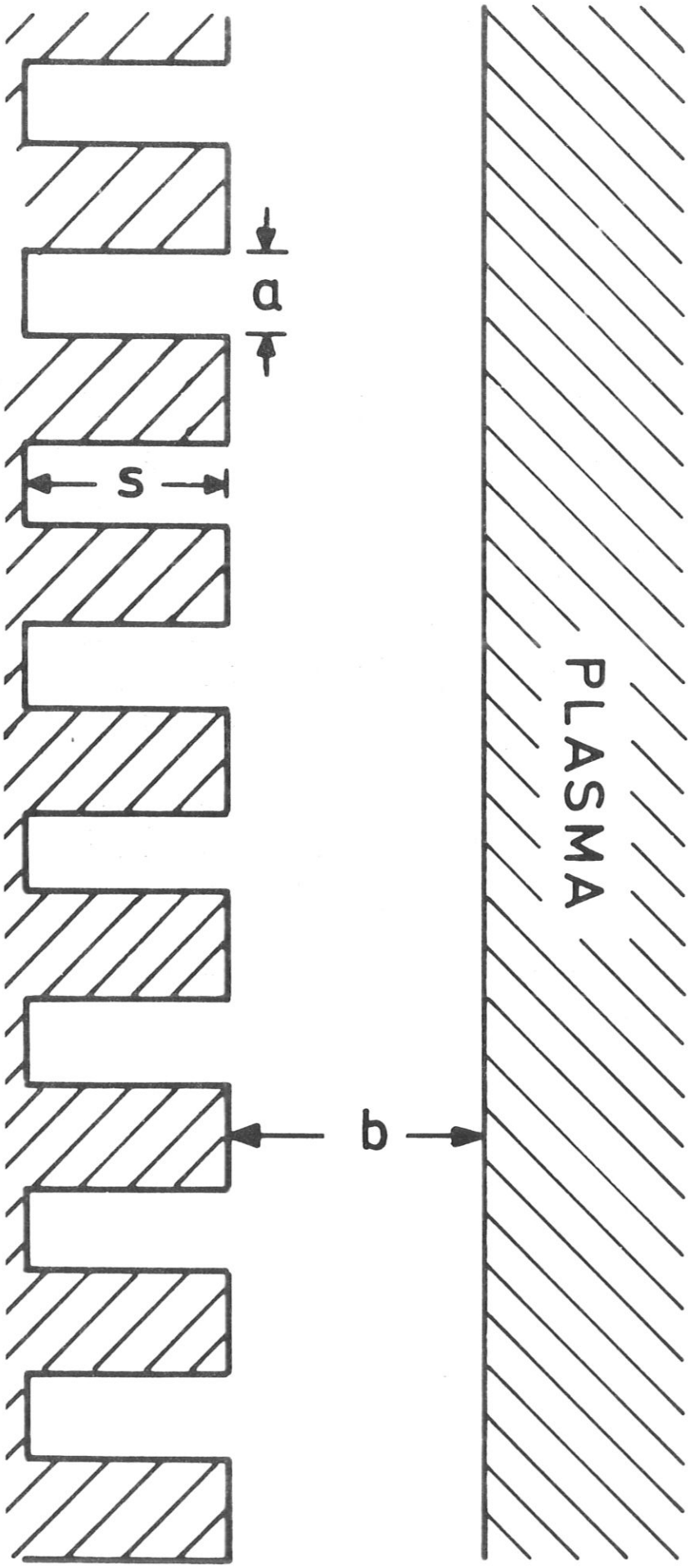

Fig. 1

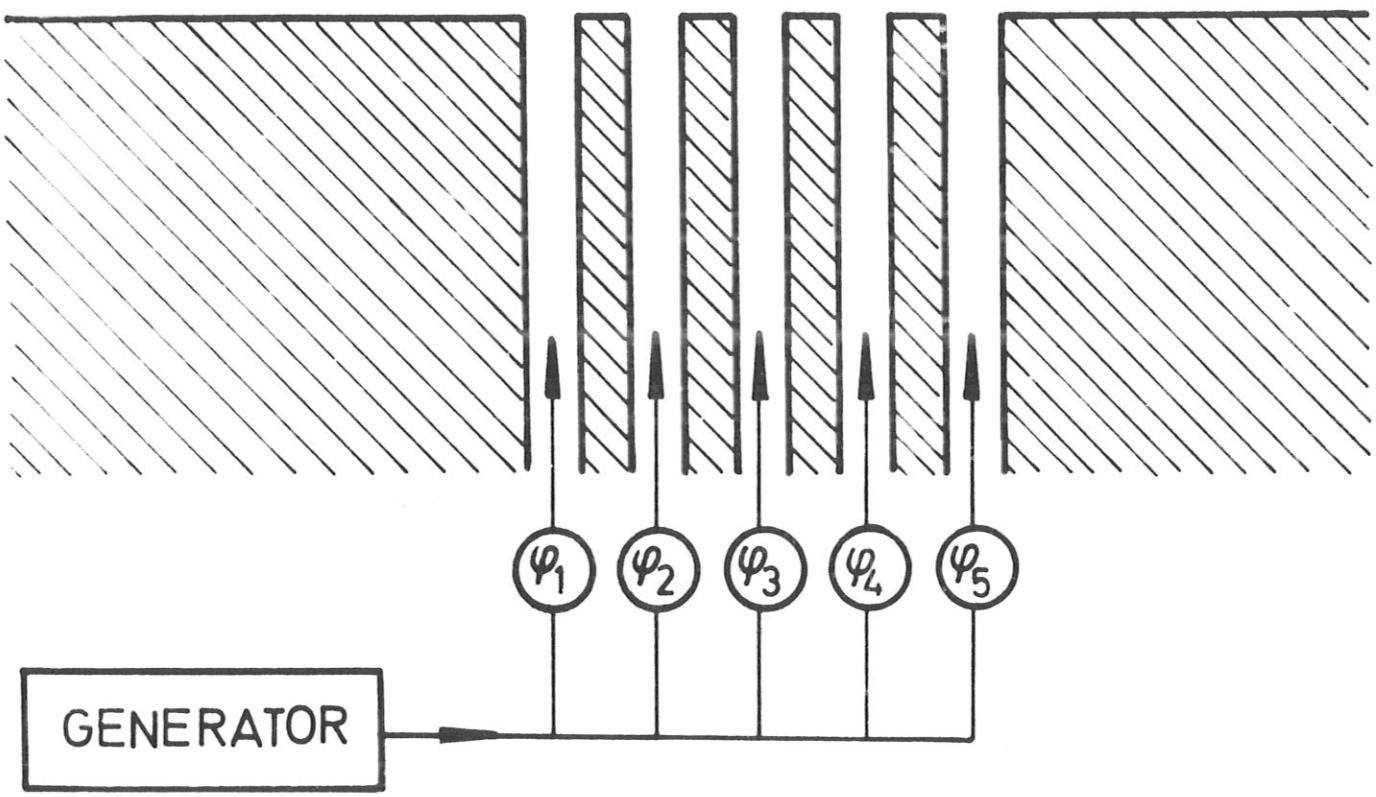

Fig. 2

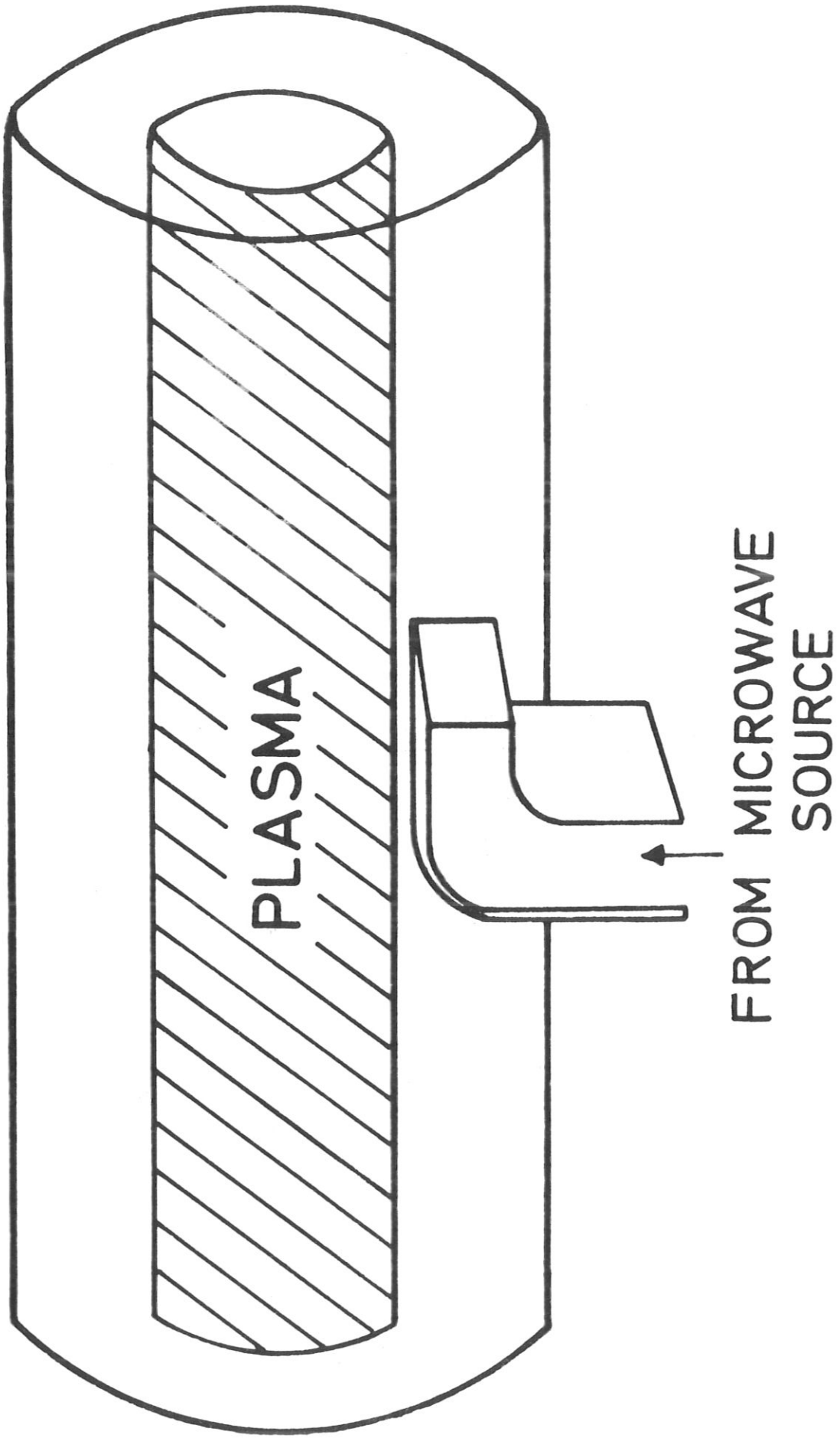

Fig. 3

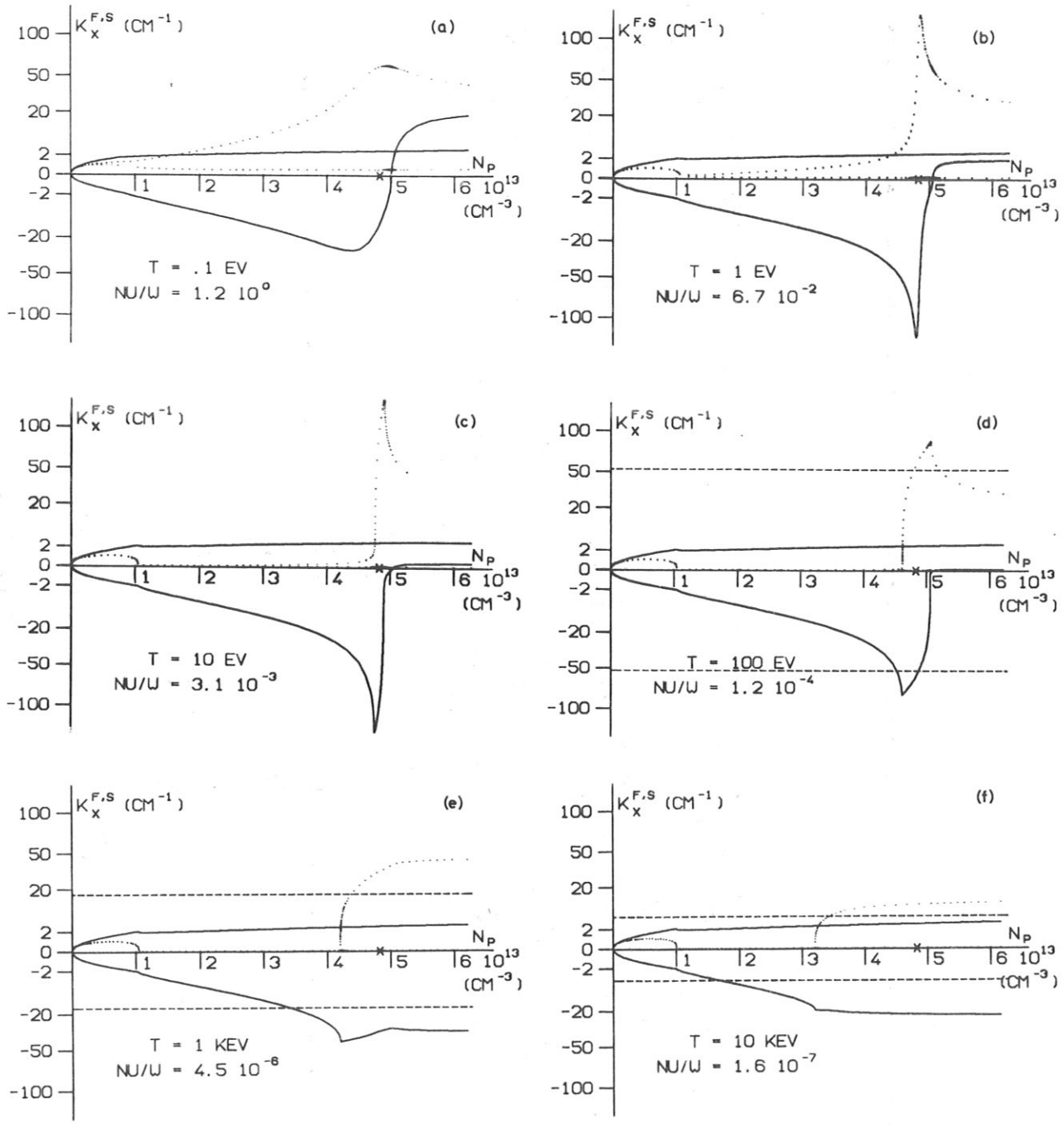
(a)
$K_x^{F,S}$ (CM^{-1})
100
50
20
2
0
-2
-20
-50
-100
1
2
3
4
5
6 10^{13}
N_P
(CM^{-3})
T = .1 EV
NU/W = 1.2 10^{0}
(b)
$K_x^{F,S}$ (CM^{-1})
T = 1 EV
NU/W = 6.7 10^{-2}
(c)
$K_x^{F,S}$ (CM^{-1})
T = 10 EV
NU/W = 3.1 10^{-3}
(d)
$K_x^{F,S}$ (CM^{-1})
T = 100 EV
NU/W = 1.2 10^{-4}
(e)
$K_x^{F,S}$ (CM^{-1})
T = 1 KEV
NU/W = 4.5 10^{-6}
(f)
$K_x^{F,S}$ (CM^{-1})
T = 10 KEV
NU/W = 1.6 10^{-7}

Fig. 4

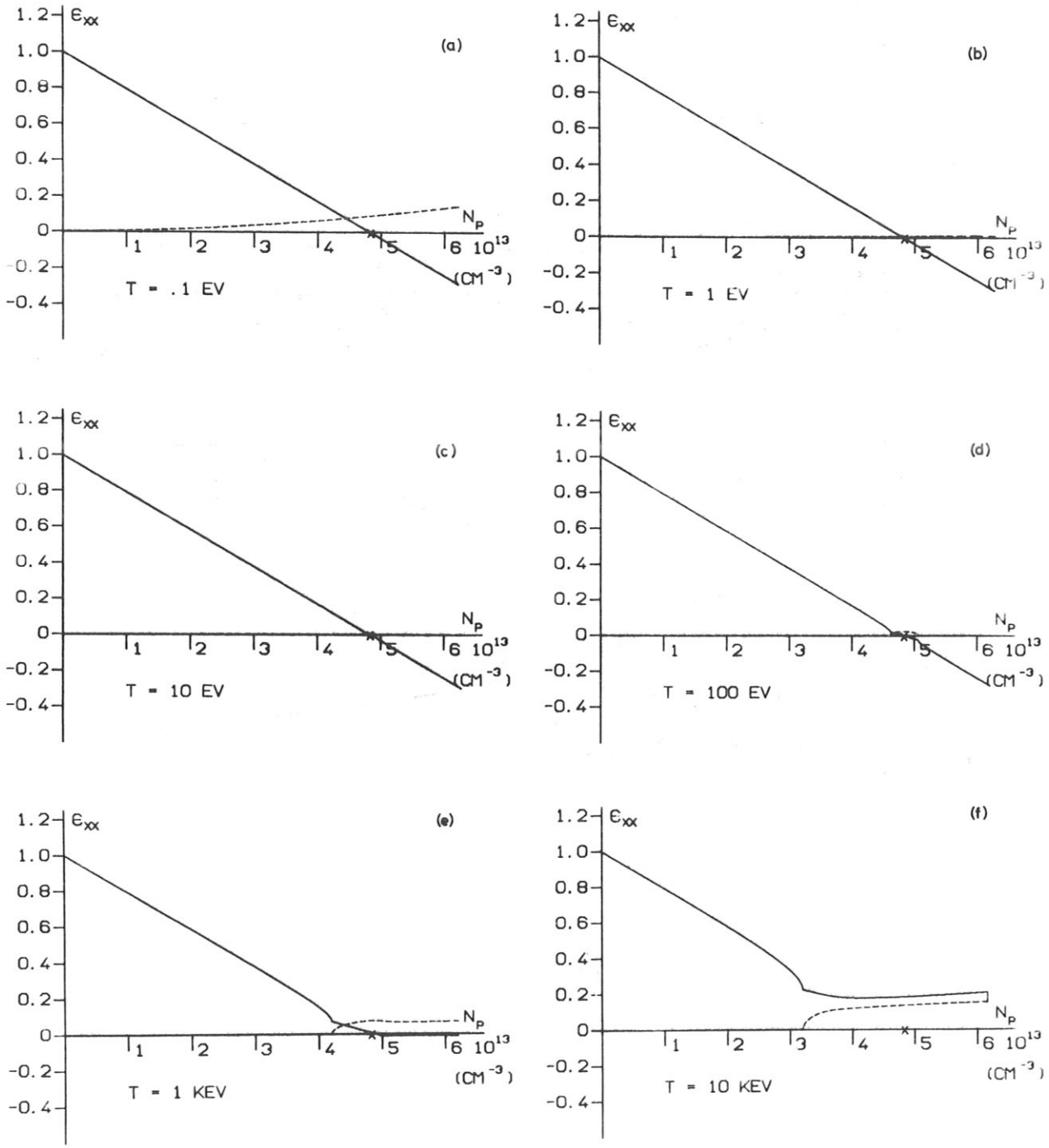
1.2
1.0
0.8
0.6
0.4
0.2
0
-0.2
-0.4
ϵ_{xx}
(a)
T = .1 EV
(b)
T = 1 EV
(c)
T = 10 EV
(d)
T = 100 EV
(e)
T = 1 KEV
(f)
T = 10 KEV
N_p
1
2
3
4
5
6 10^{13}
(CM^{-3})

Fig. 5

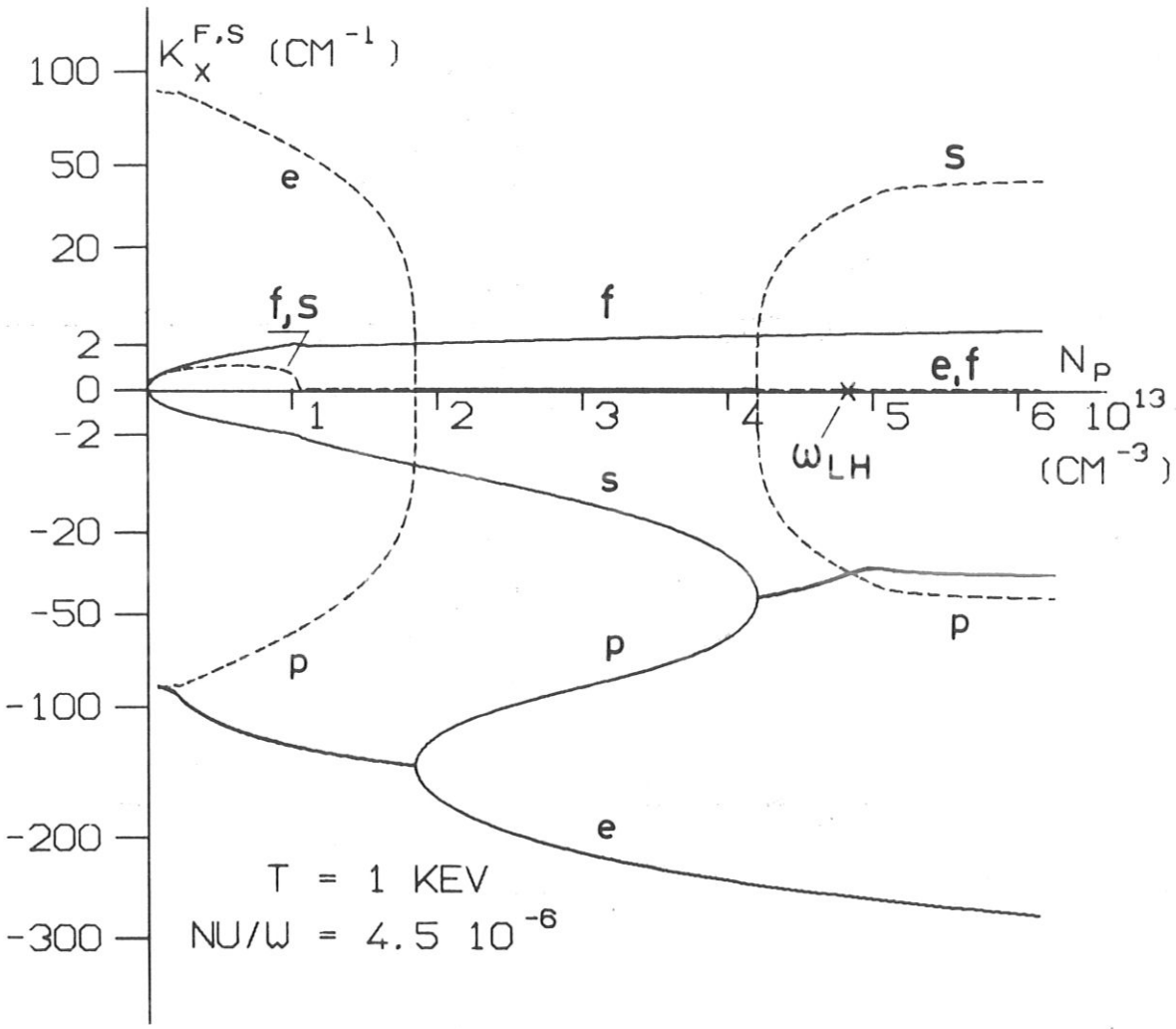
$K_x^{F,S}$ (CM^{-1})
100
50
20
2
0
-2
-20
-50
-100
-200
-300
e
s
f,s
f
e,f
N_P
1
2
3
4
5
6 10^{13}
(CM^{-3})
ω_{LH}
s
p
p
p
e
T = 1 KEV
NU/W = 4.5 10^{-6}

Fig. 6

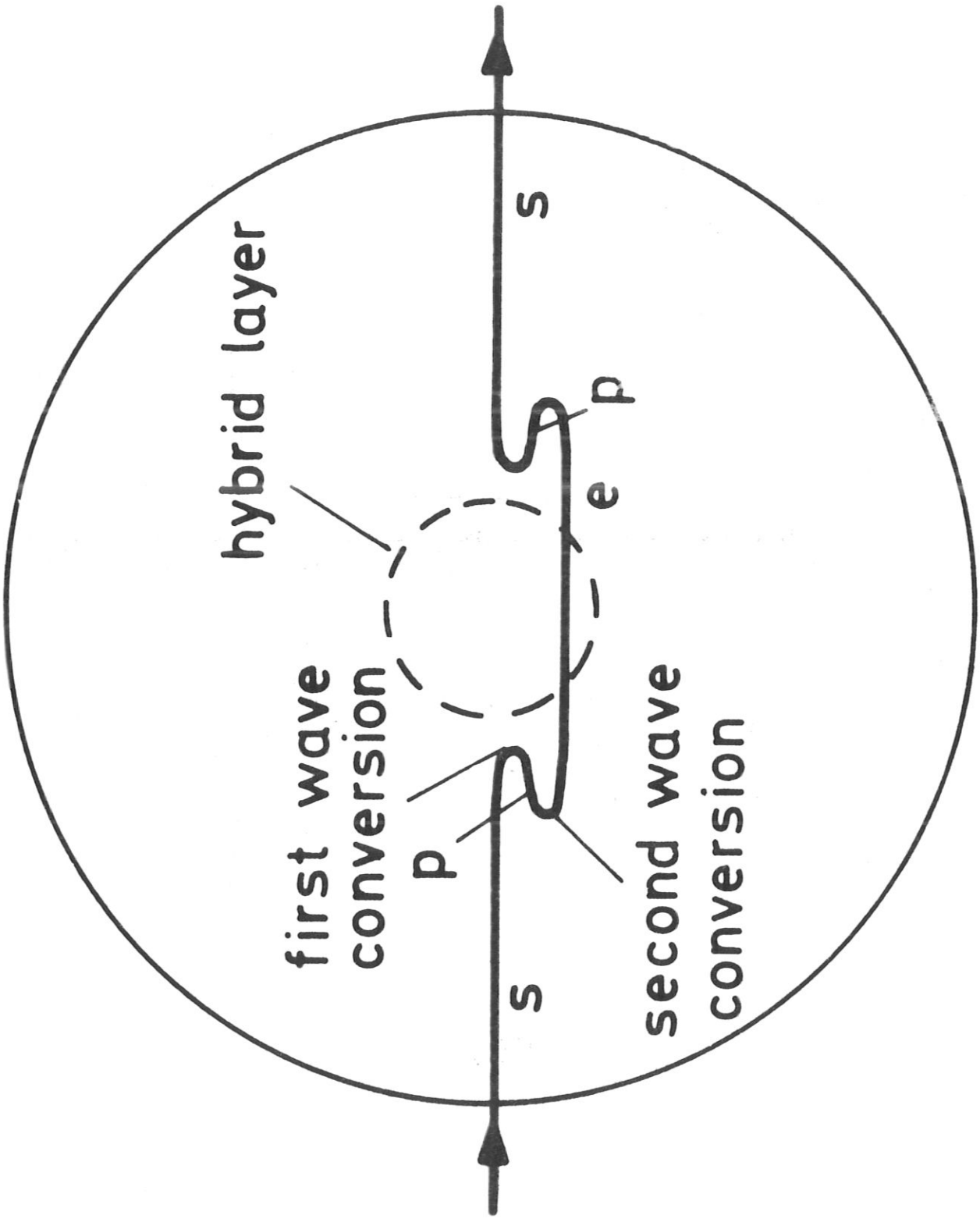
hybrid layer
first wave conversion
second wave conversion
s
p
e
p
s

Fig. 7

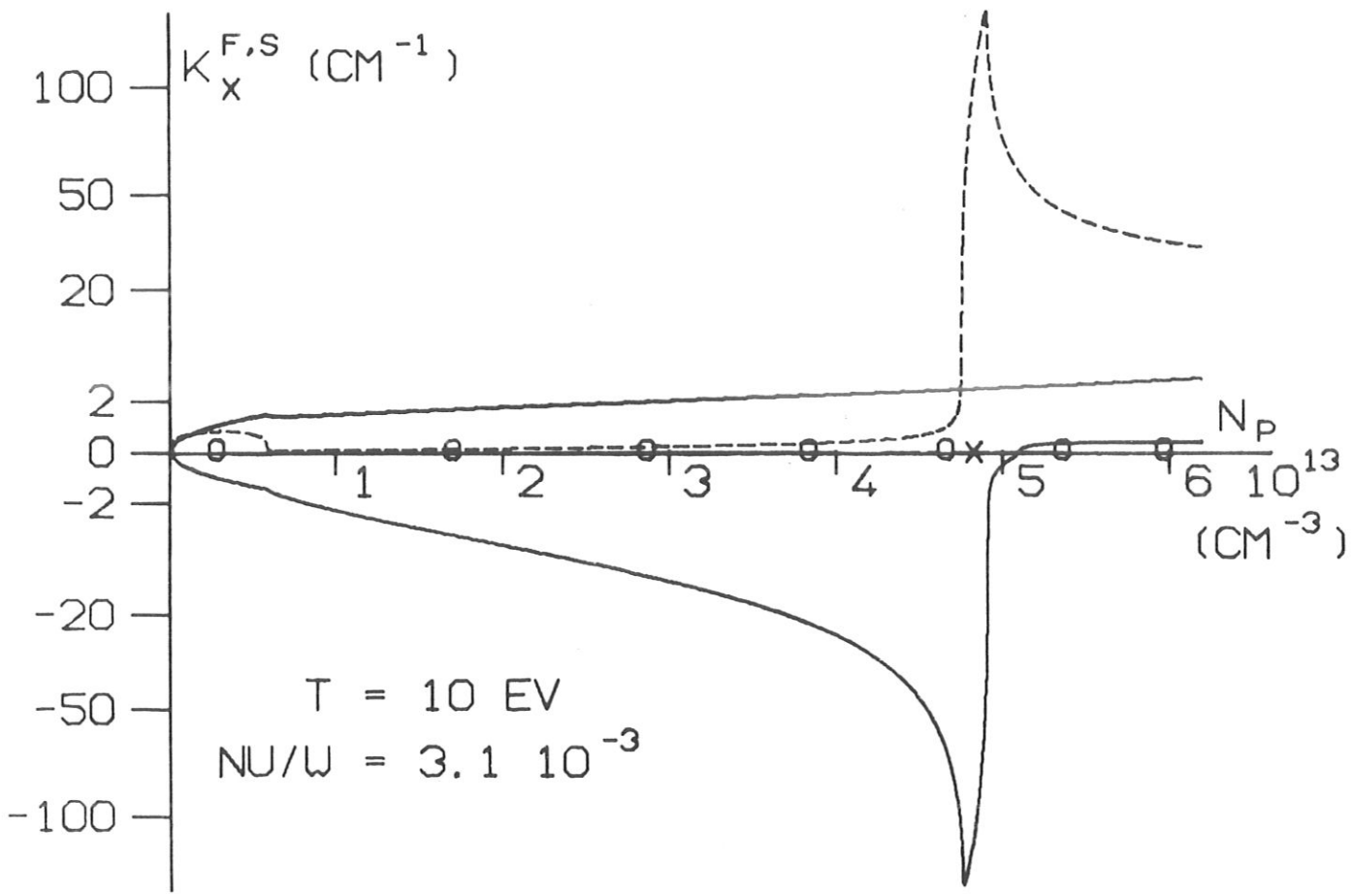
$K_x^{F,S}$ (CM^{-1})
100
50
20
2
0
-2
-20
-50
-100
1
2
3
4
5
6
10^{13}
N_P
(CM^{-3})
T = 10 EV
NU/W = 3.1 10^{-3}

Fig. 8

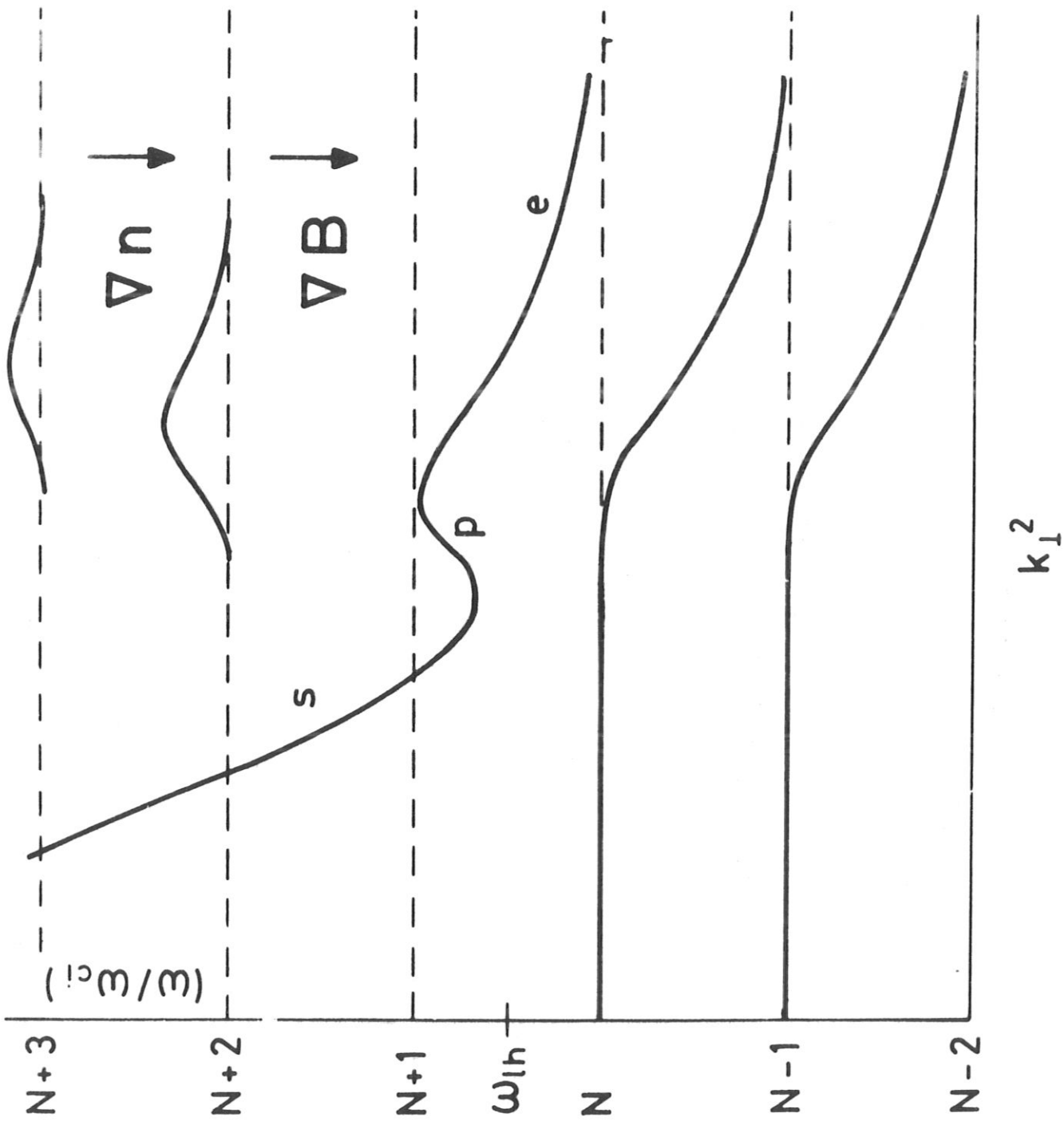

Fig. 9a

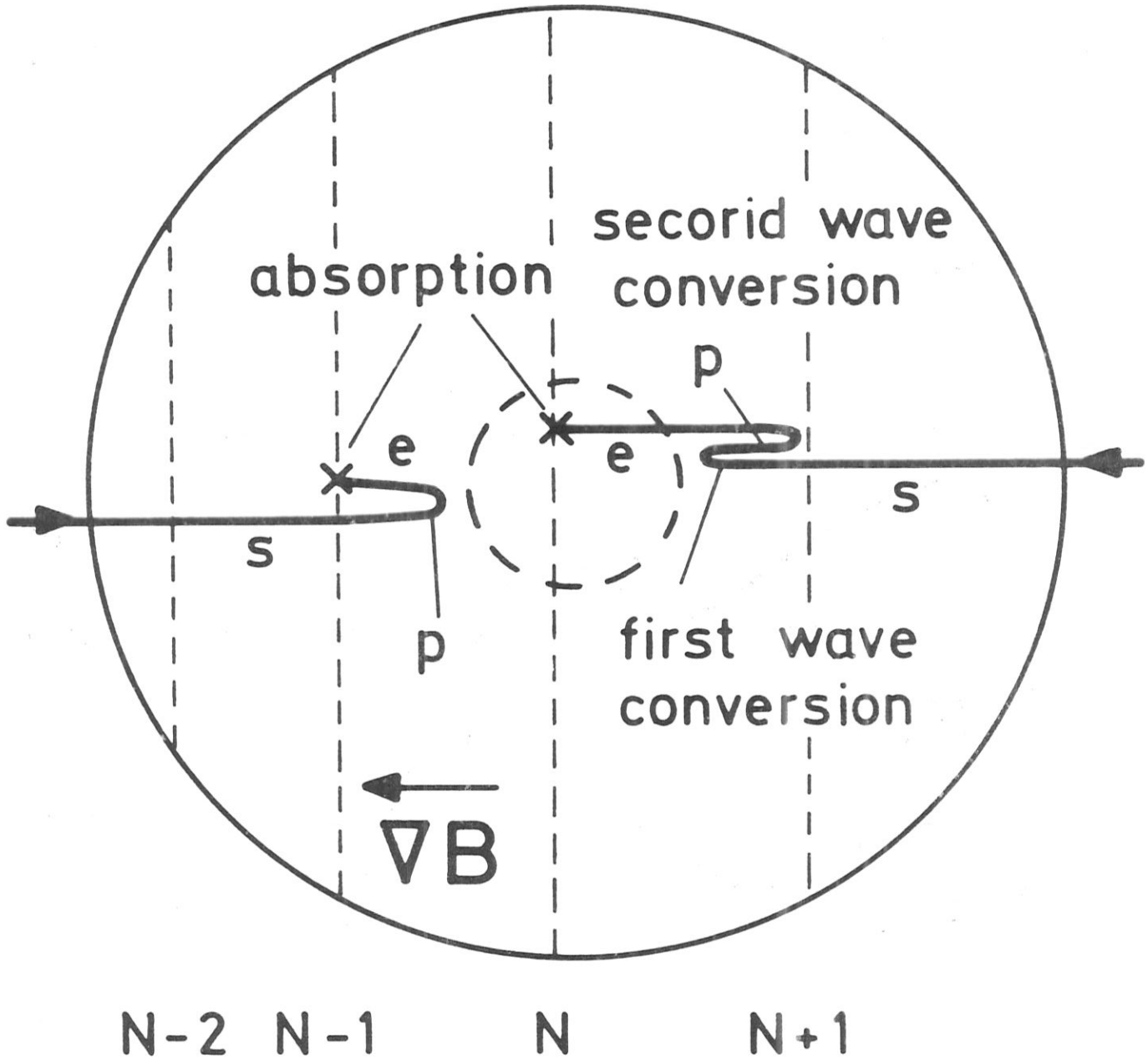
absorption
secorid wave
conversion
p
e
e
s
s
p
first wave
conversion
∇B
N-2
N-1
N
N+1

Fig. 9b

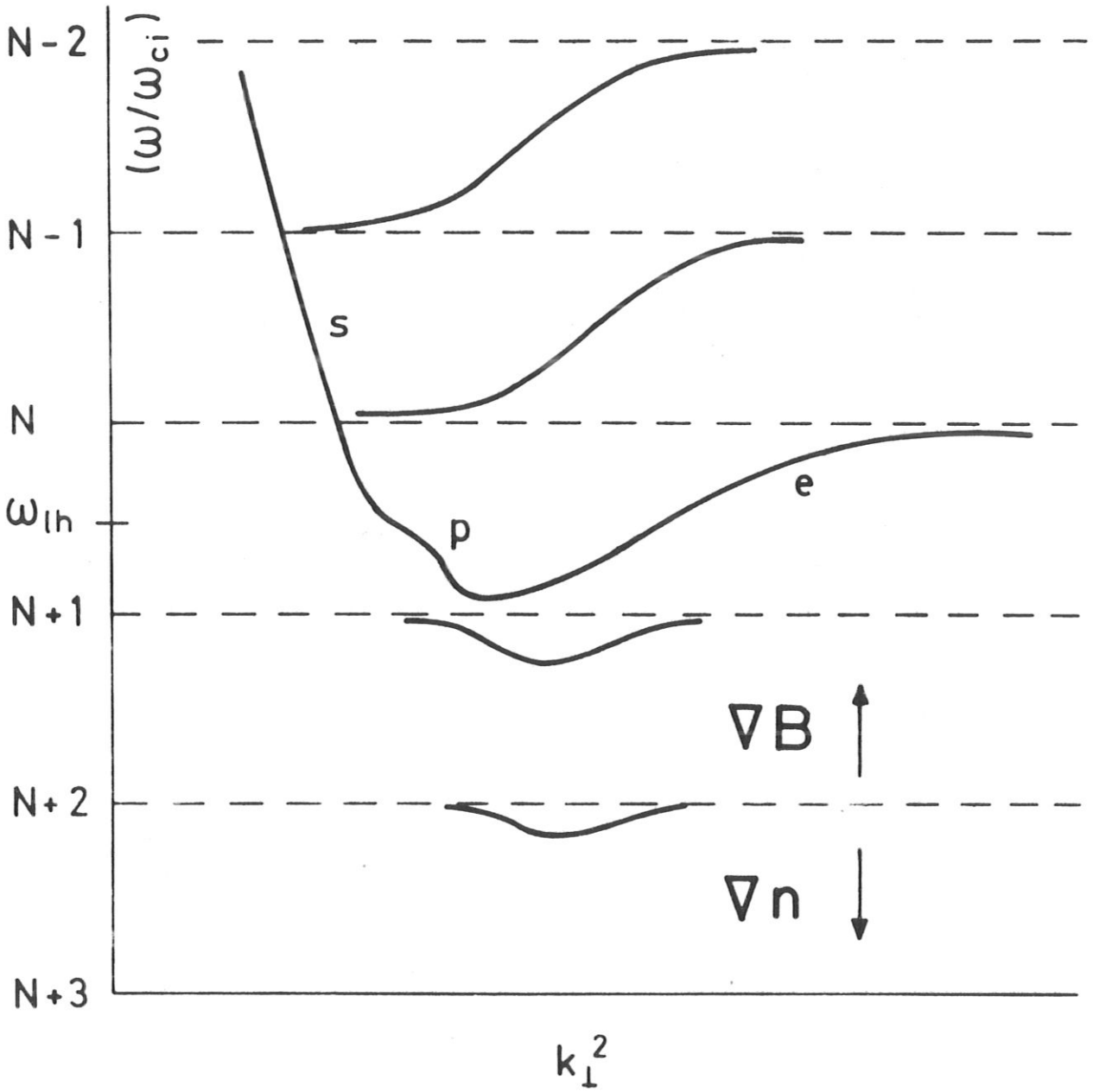
N-2
N-1
N
ω_{lh}
N+1
N+2
N+3
(ω/ω_{ci})
s
p
e
∇B
∇n
$k_\perp^2$

Fig. 10

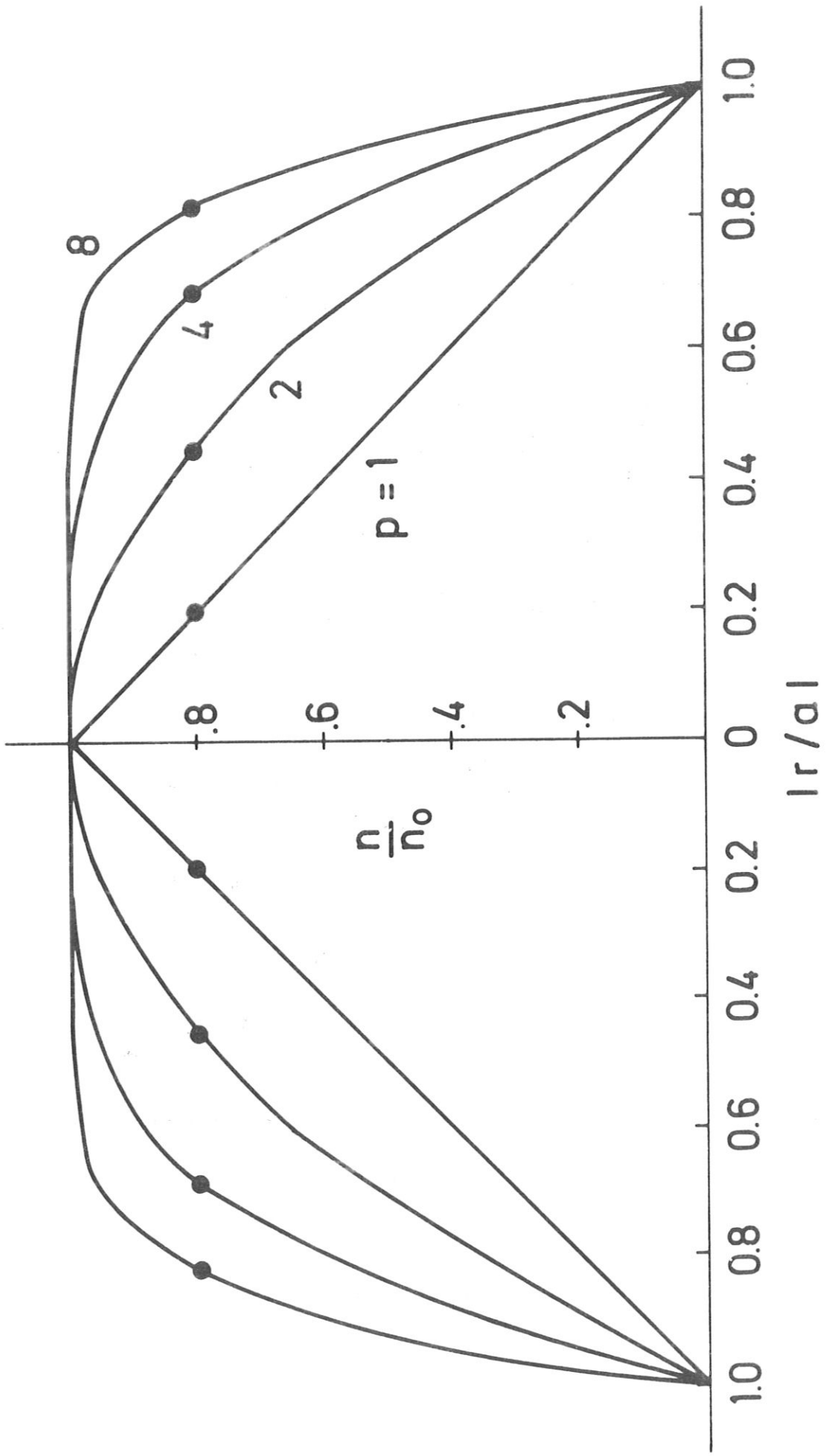

Fig. 11

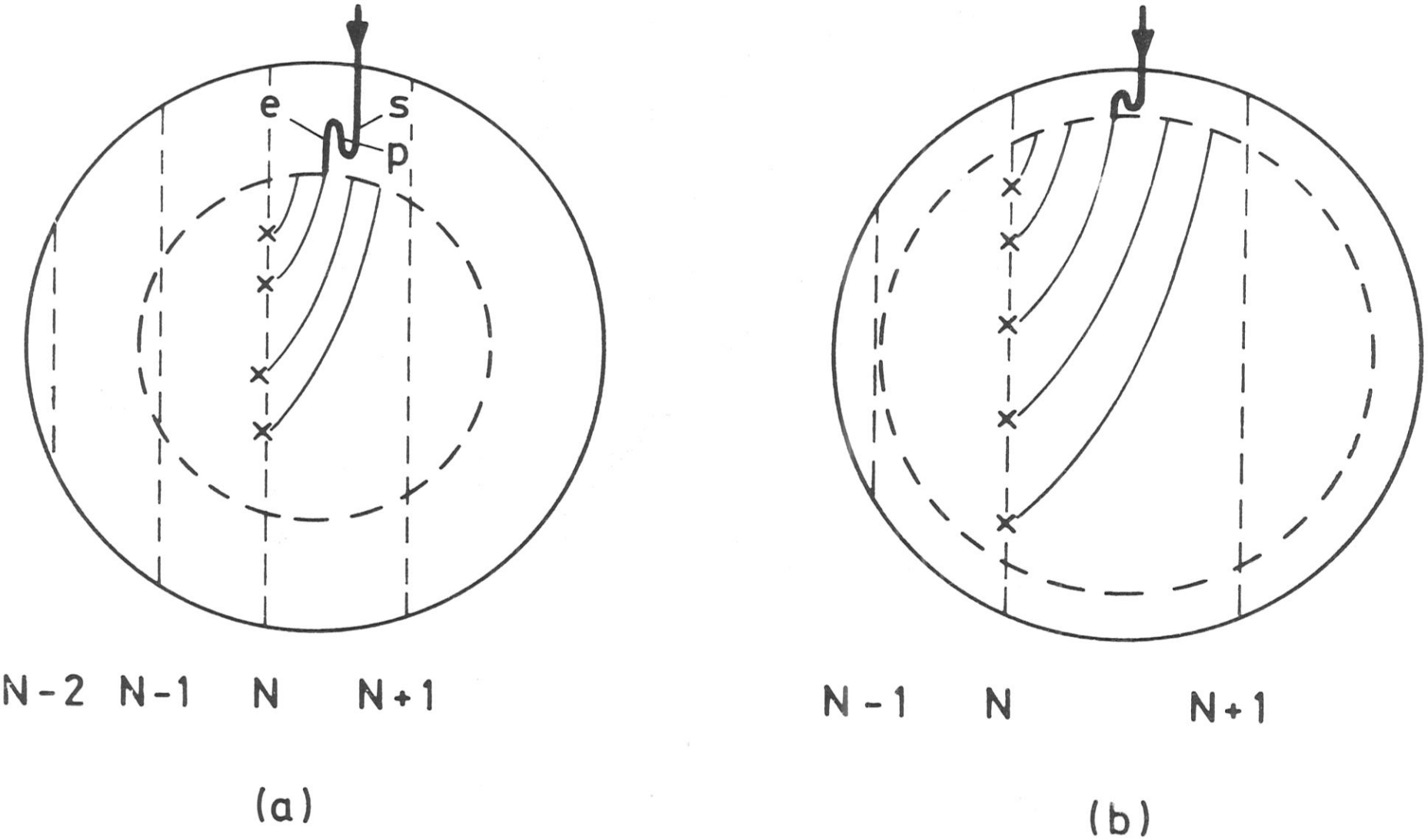

Fig. 12

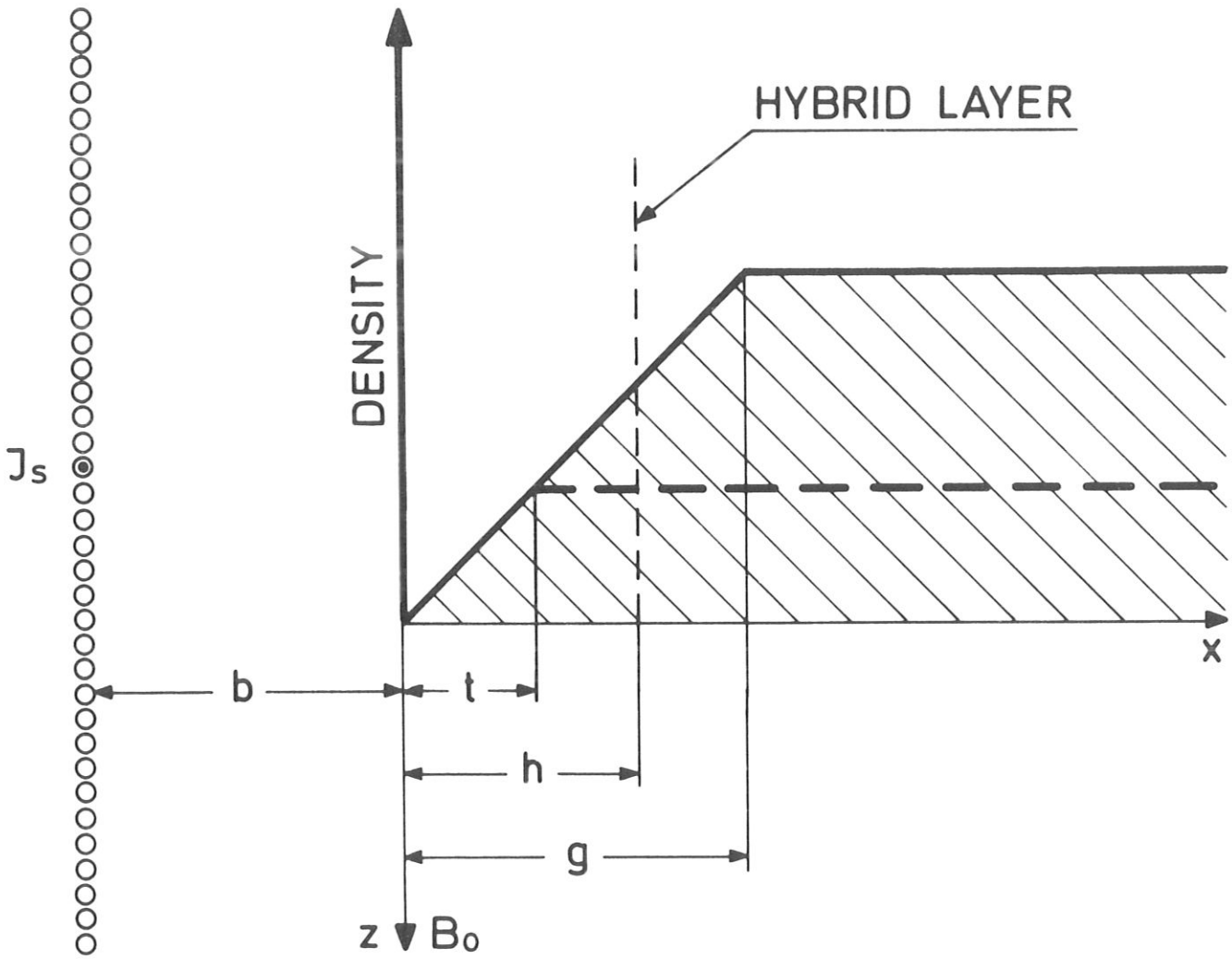

Fig. 13

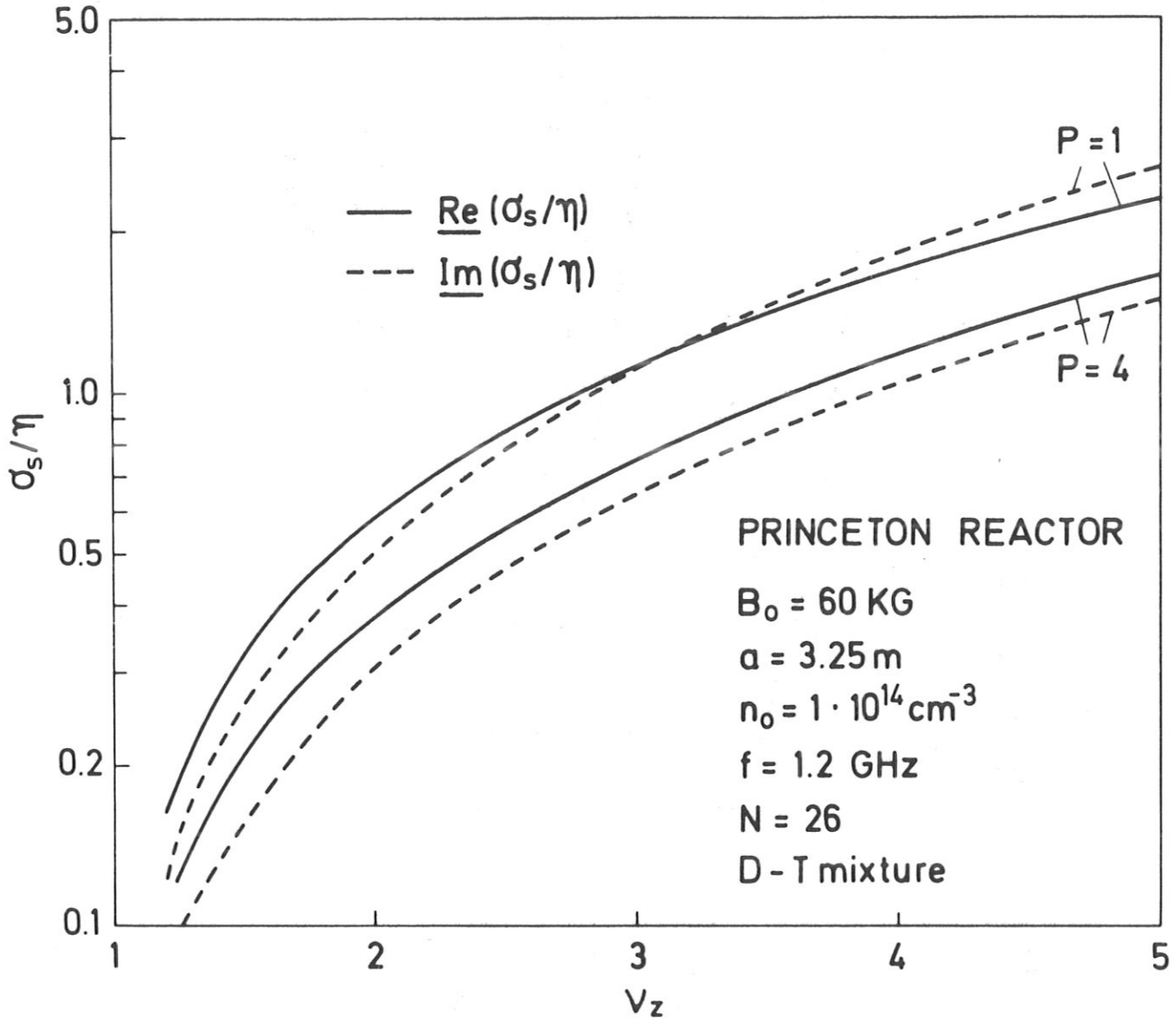
5.0
1.0
0.5
0.2
0.1
1
2
3
4
5
σ_s/η
ν_z
Re (σ_s/η)
Im (σ_s/η)
P = 1
P = 4
PRINCETON REACTOR
B_o = 60 KG
a = 3.25 m
$n_o = 1 \cdot 10^{14}\,cm^{-3}$
f = 1.2 GHz
N = 26
D - T mixture

Fig. 14

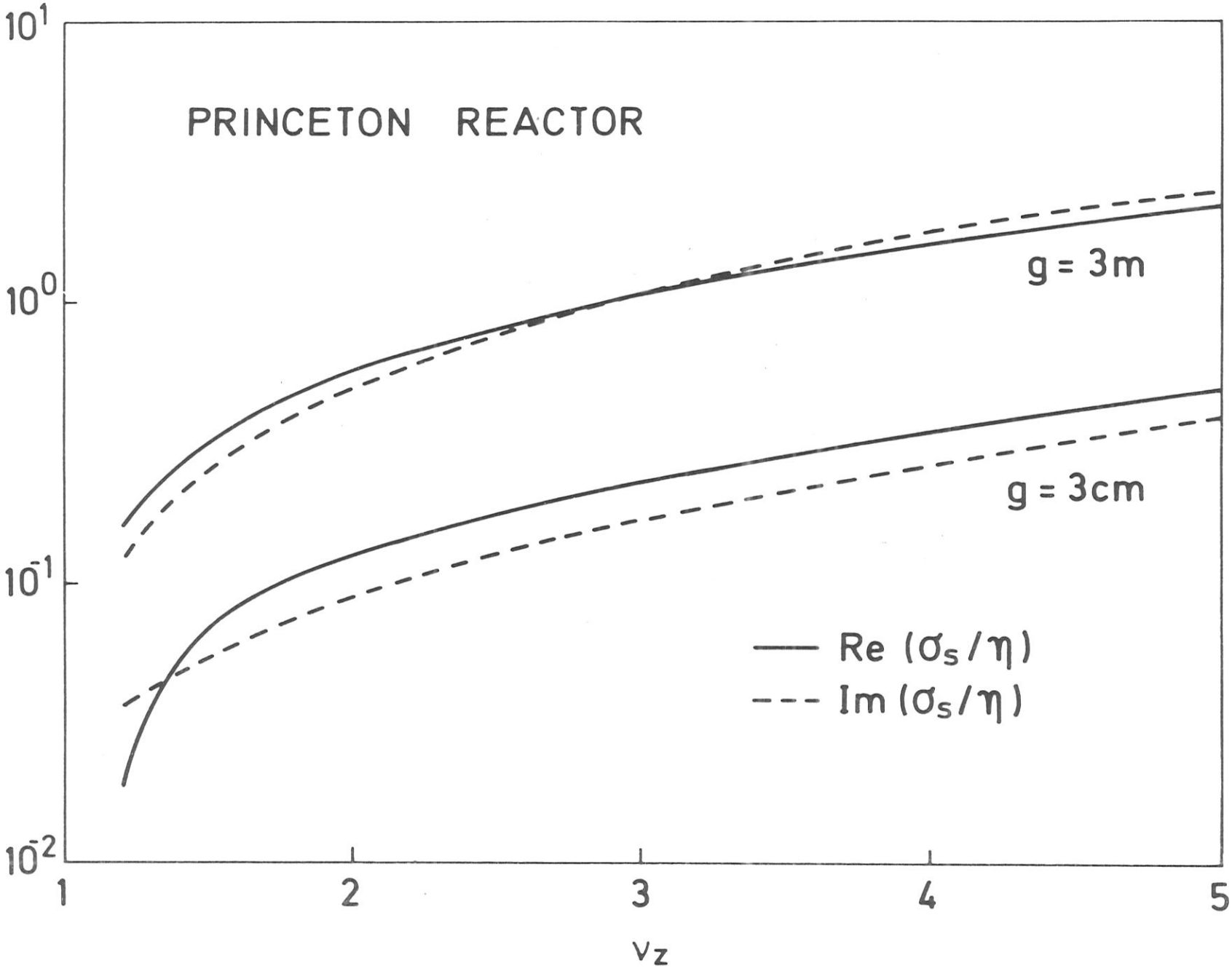
PRINCETON REACTOR
g = 3m
g = 3cm
Re (σs/η)
Im (σs/η)
σs/η
νz
10^1
10^0
10^-1
10^-2
1
2
3
4
5

Fig. 15

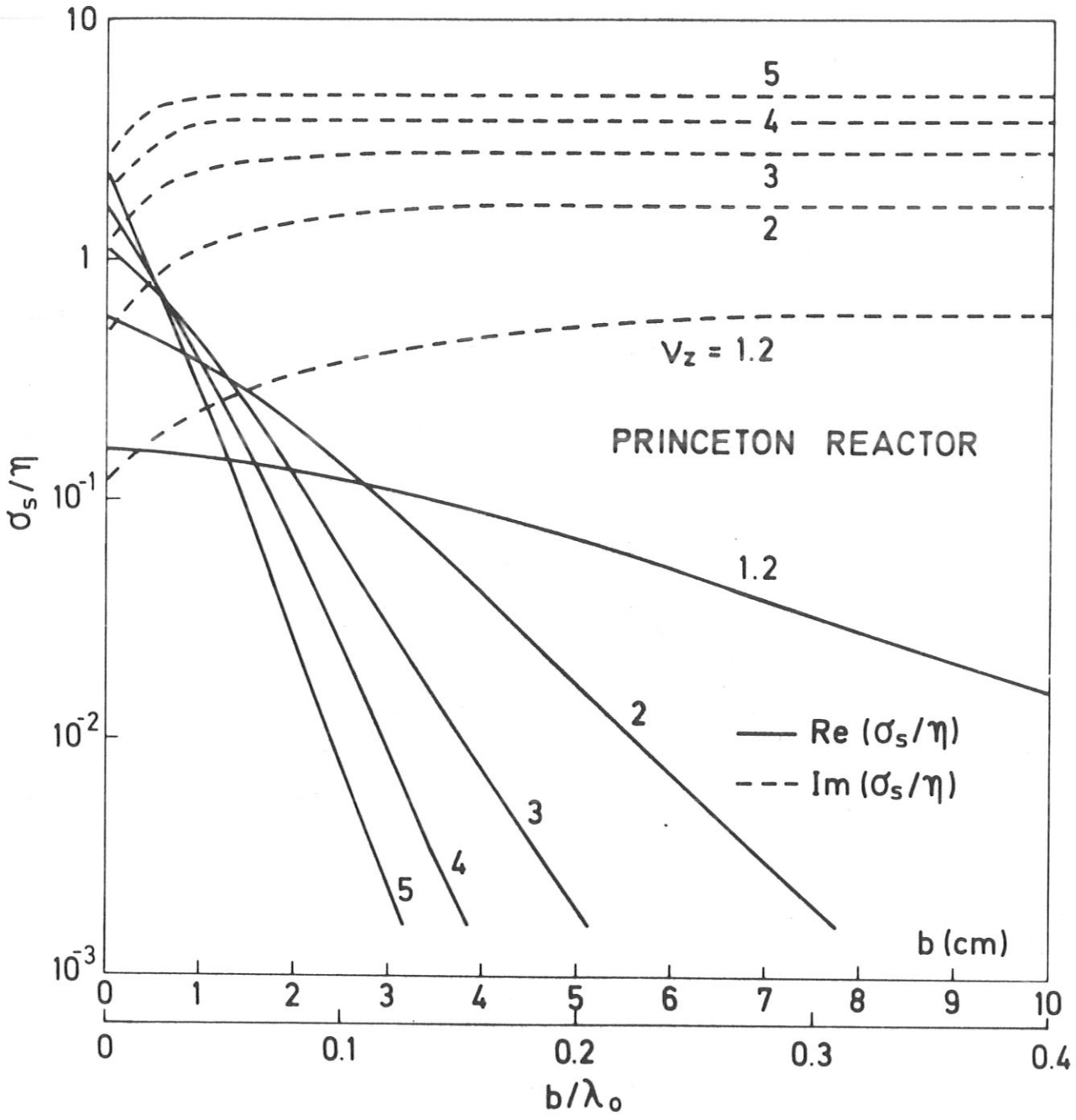
10
1
10^{-1}
10^{-2}
10^{-3}
σ_s/η
5
4
3
2
V_z = 1.2
PRINCETON REACTOR
1.2
2
3
4
5
Re (σ_s/η)
Im (σ_s/η)
b (cm)
0 1 2 3 4 5 6 7 8 9 10
0 0.1 0.2 0.3 0.4
b/λ_o

Fig. 16

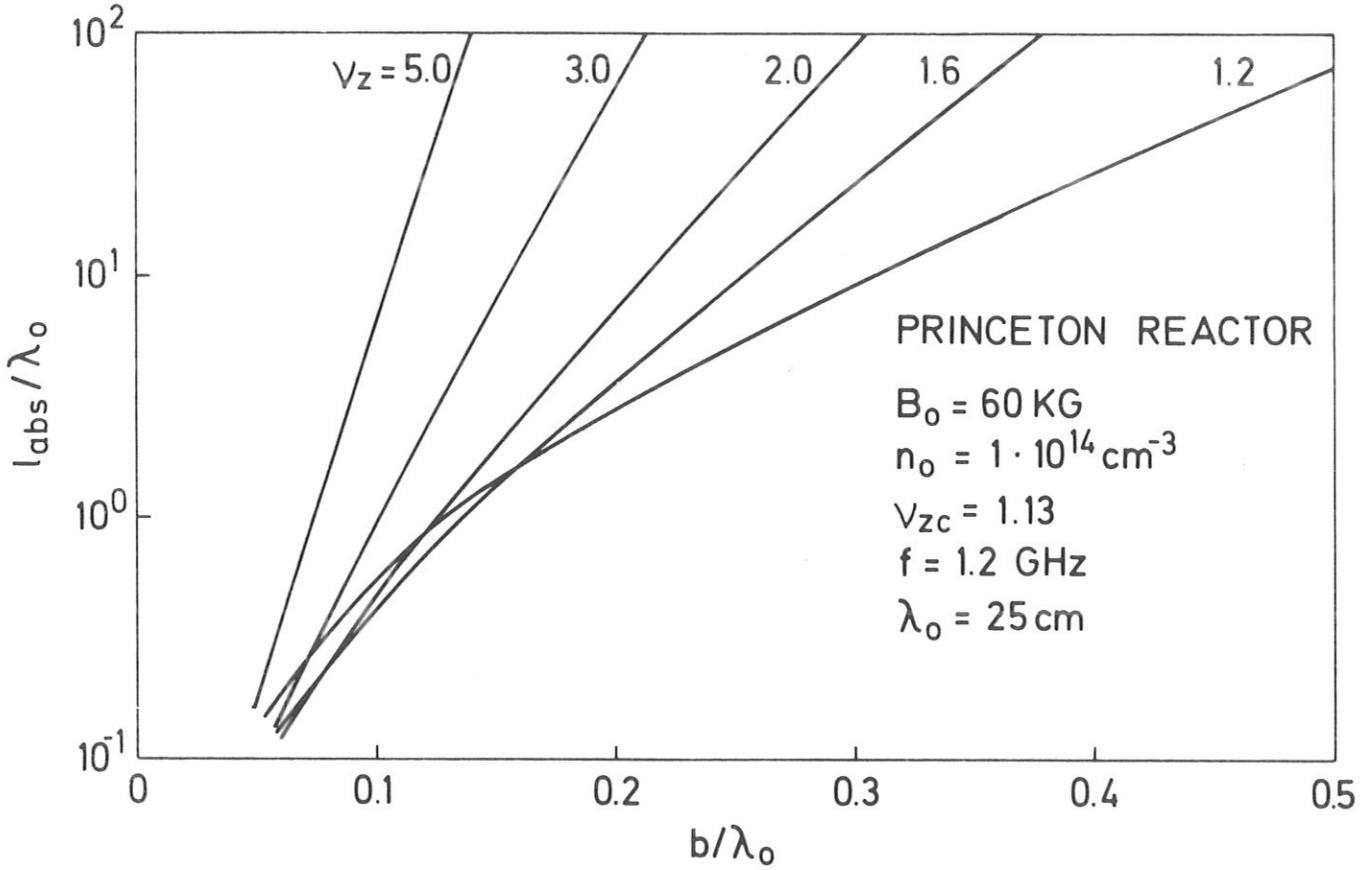
10^2
10^1
10^0
10^{-1}
l_{abs}/λ_o
$v_z = 5.0$
3.0
2.0
1.6
1.2
PRINCETON REACTOR
$B_o = 60\,KG$
$n_o = 1 \cdot 10^{14}\,cm^{-3}$
$v_{zc} = 1.13$
$f = 1.2\,GHz$
$\lambda_o = 25\,cm$
0
0.1
0.2
0.3
0.4
0.5
b/λ_o

Fig. 17

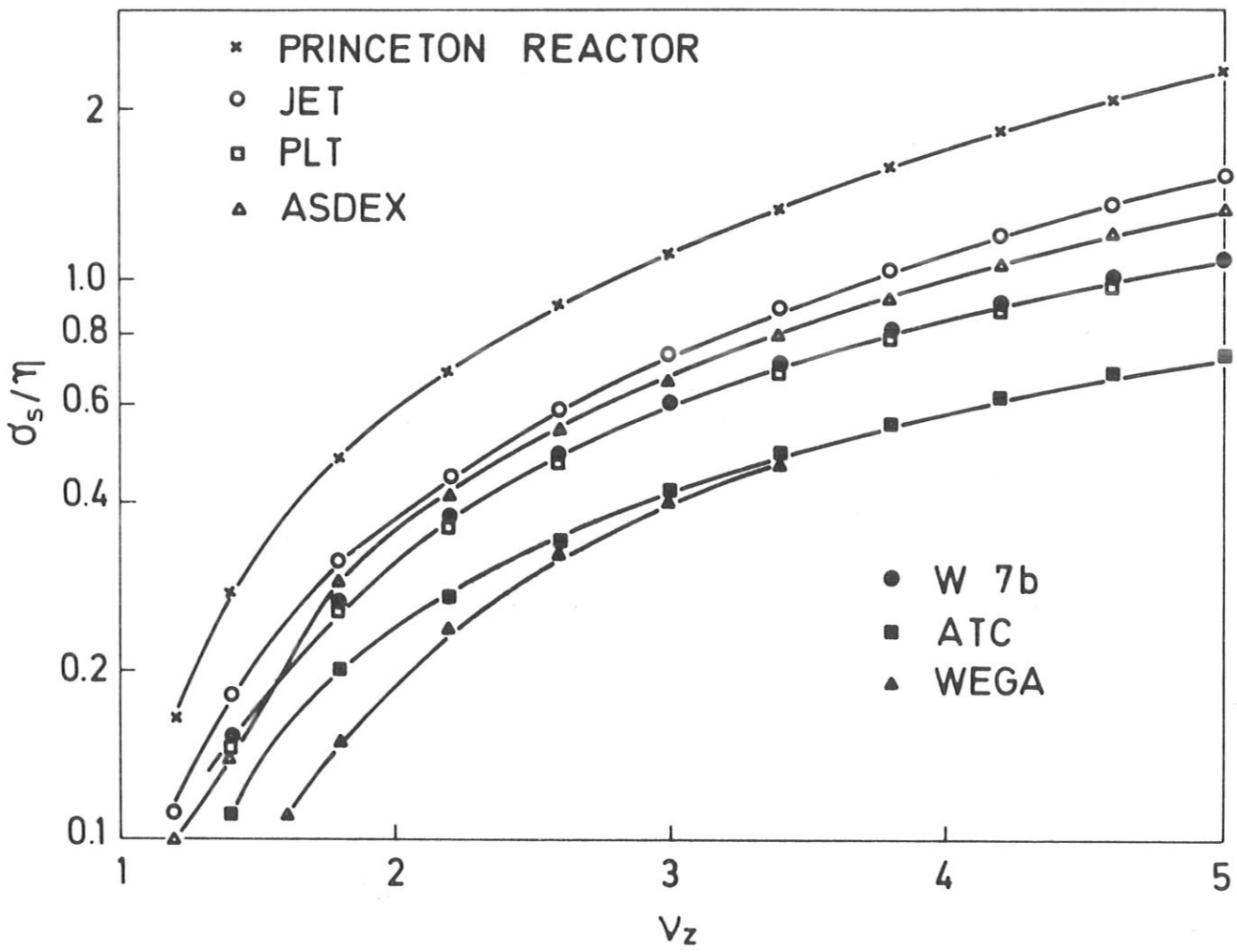
PRINCETON REACTOR
JET
PLT
ASDEX
W 7b
ATC
WEGA
2
1.0
0.8
0.6
0.4
0.2
0.1
σ_s/η
1
2
3
4
5
ν_z

Fig. 18

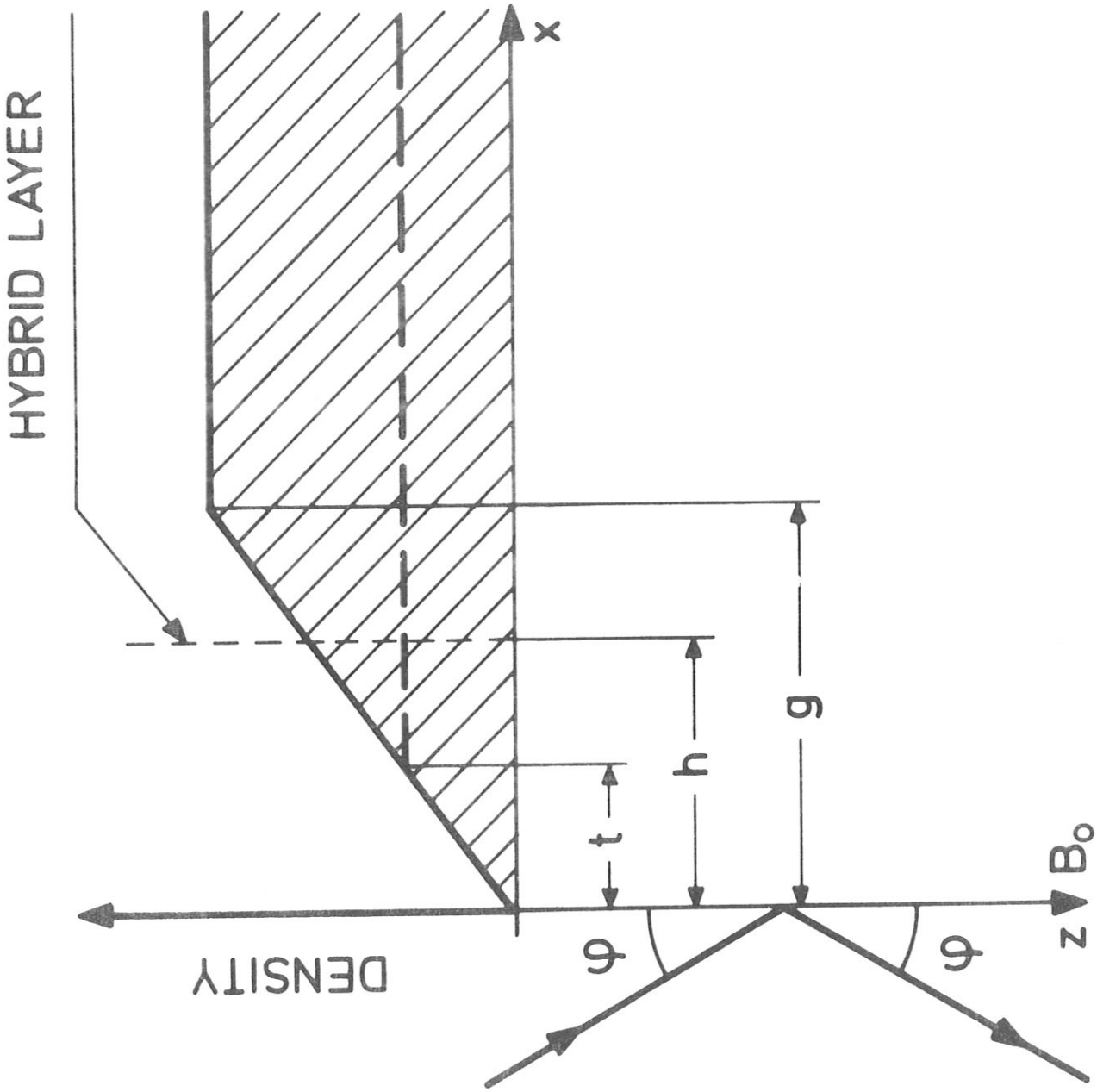

Fig. 19

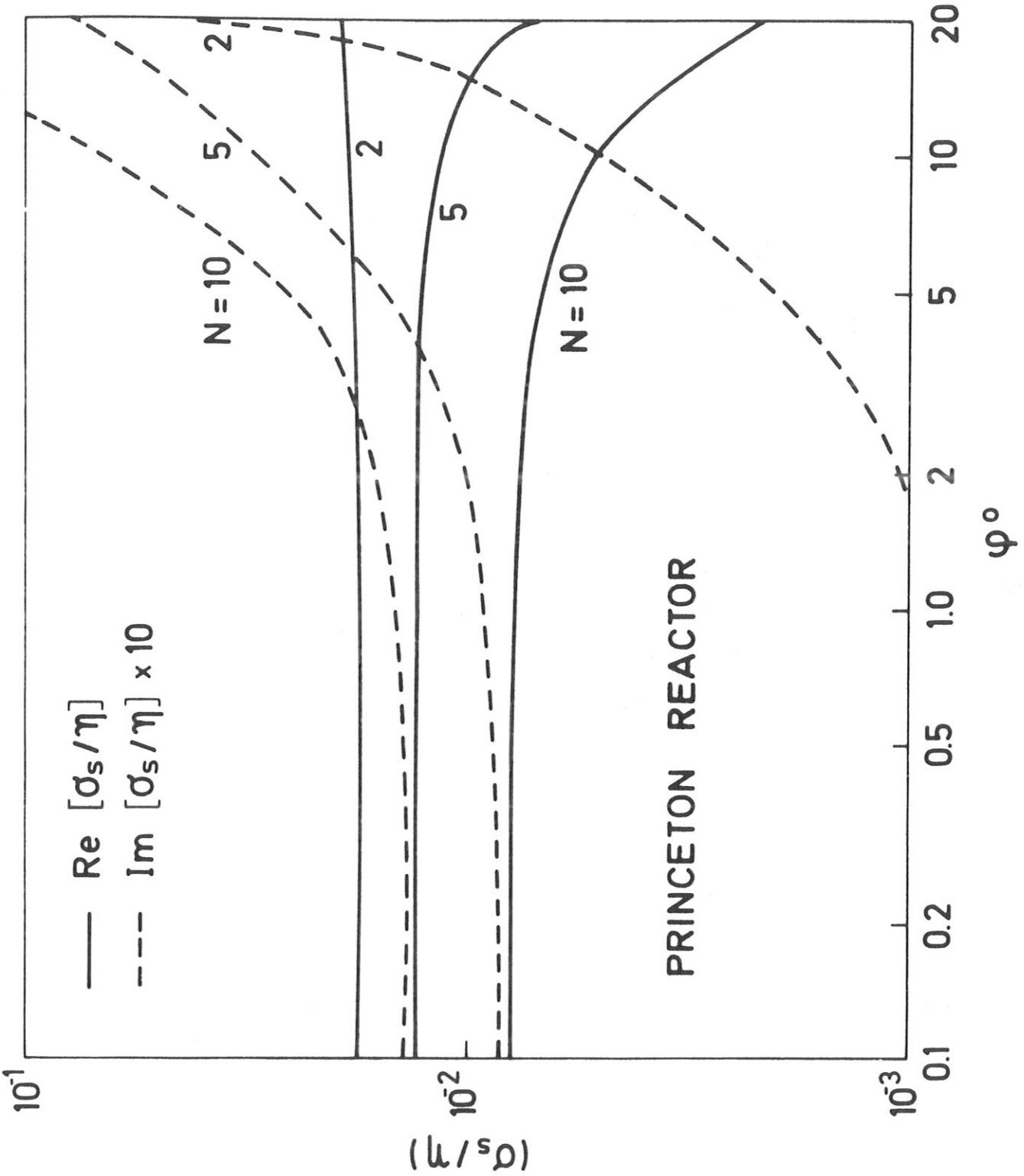
Re [σs/η]
Im [σs/η] x 10
N=10
5
2
N=10
5
2
PRINCETON REACTOR
10^-1
10^-2
10^-3
(σs/η)
0.1
0.2
0.5
1.0
2
5
10
20
φ°

Fig. 20

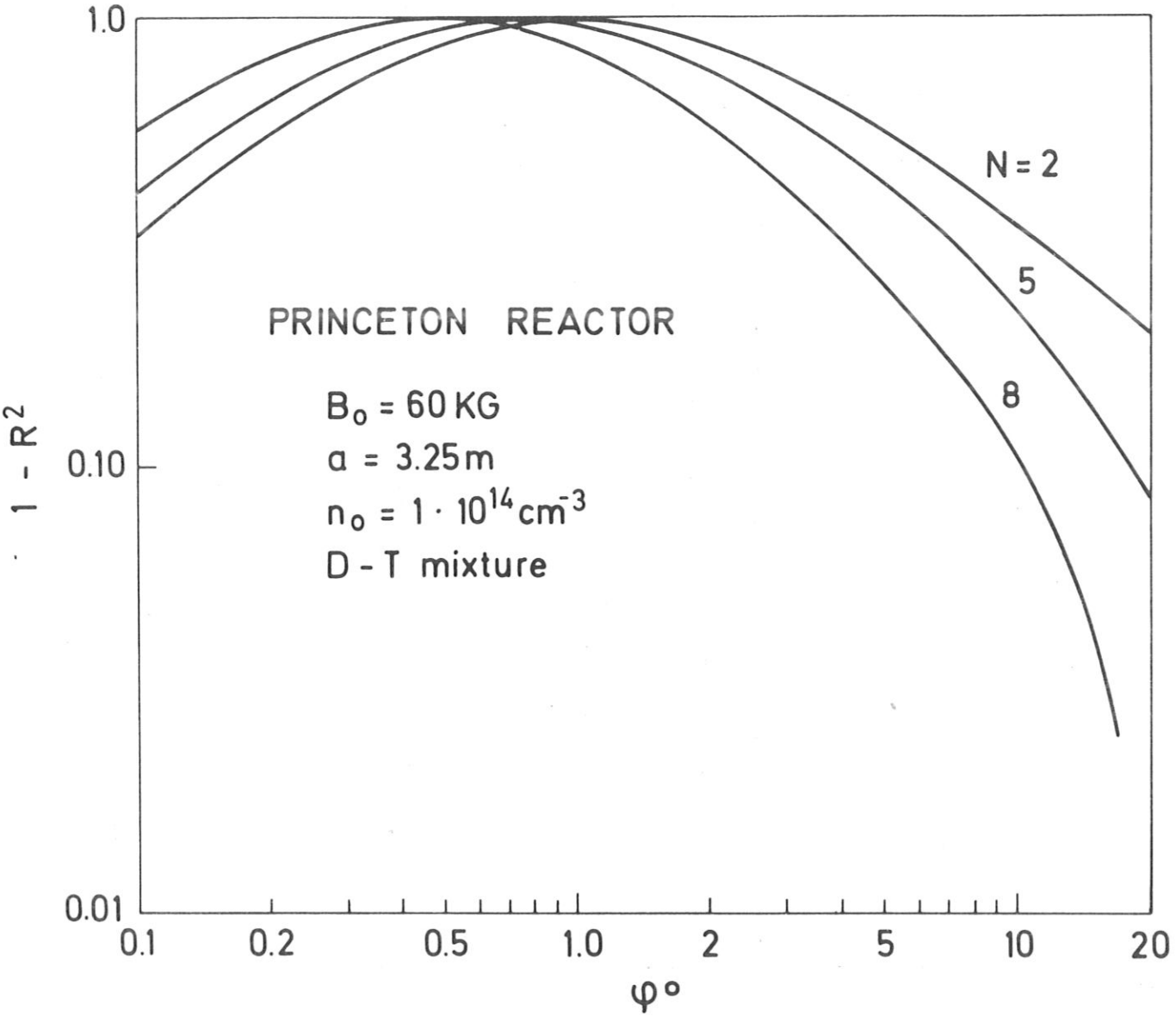
1.0
0.10
0.01
1 - R²
N = 2
5
8
PRINCETON REACTOR
B₀ = 60 KG
a = 3.25 m
n₀ = 1 · 10¹⁴ cm⁻³
D - T mixture
0.1
0.2
0.5
1.0
2
5
10
20
φ°

Fig. 21

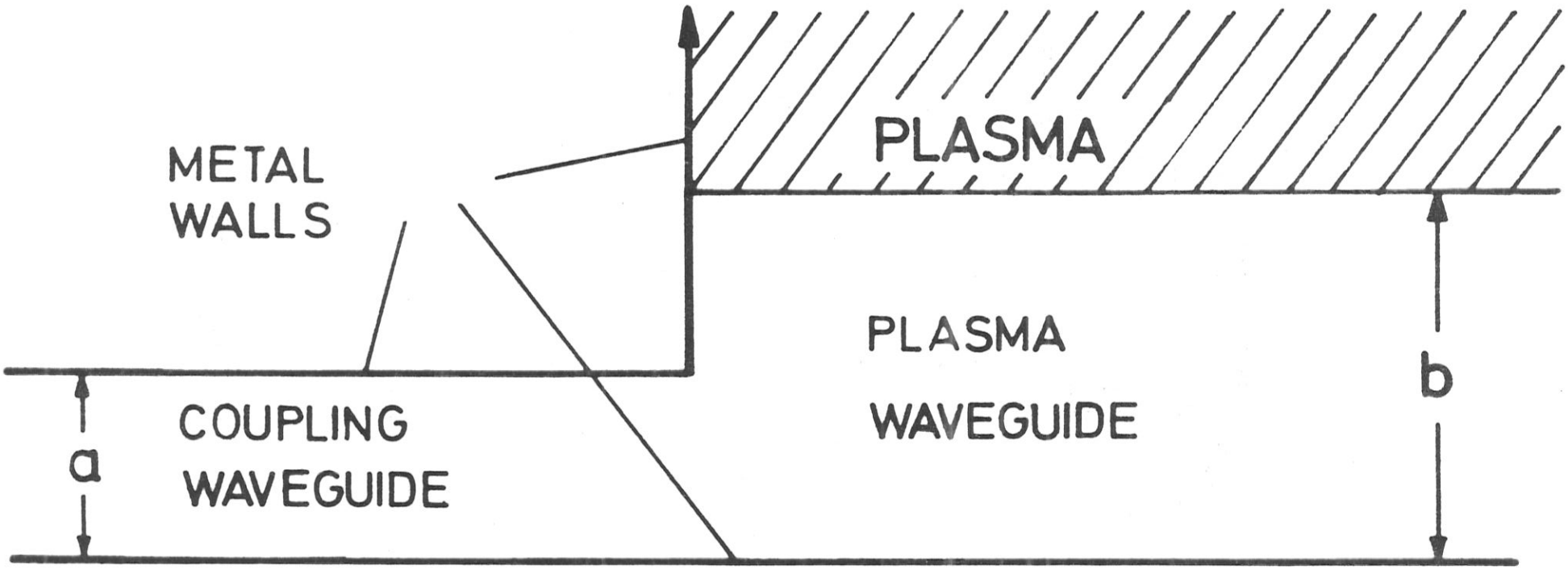
PLASMA
METAL
WALLS
PLASMA
WAVEGUIDE
b
a
COUPLING
WAVEGUIDE

Fig. 22

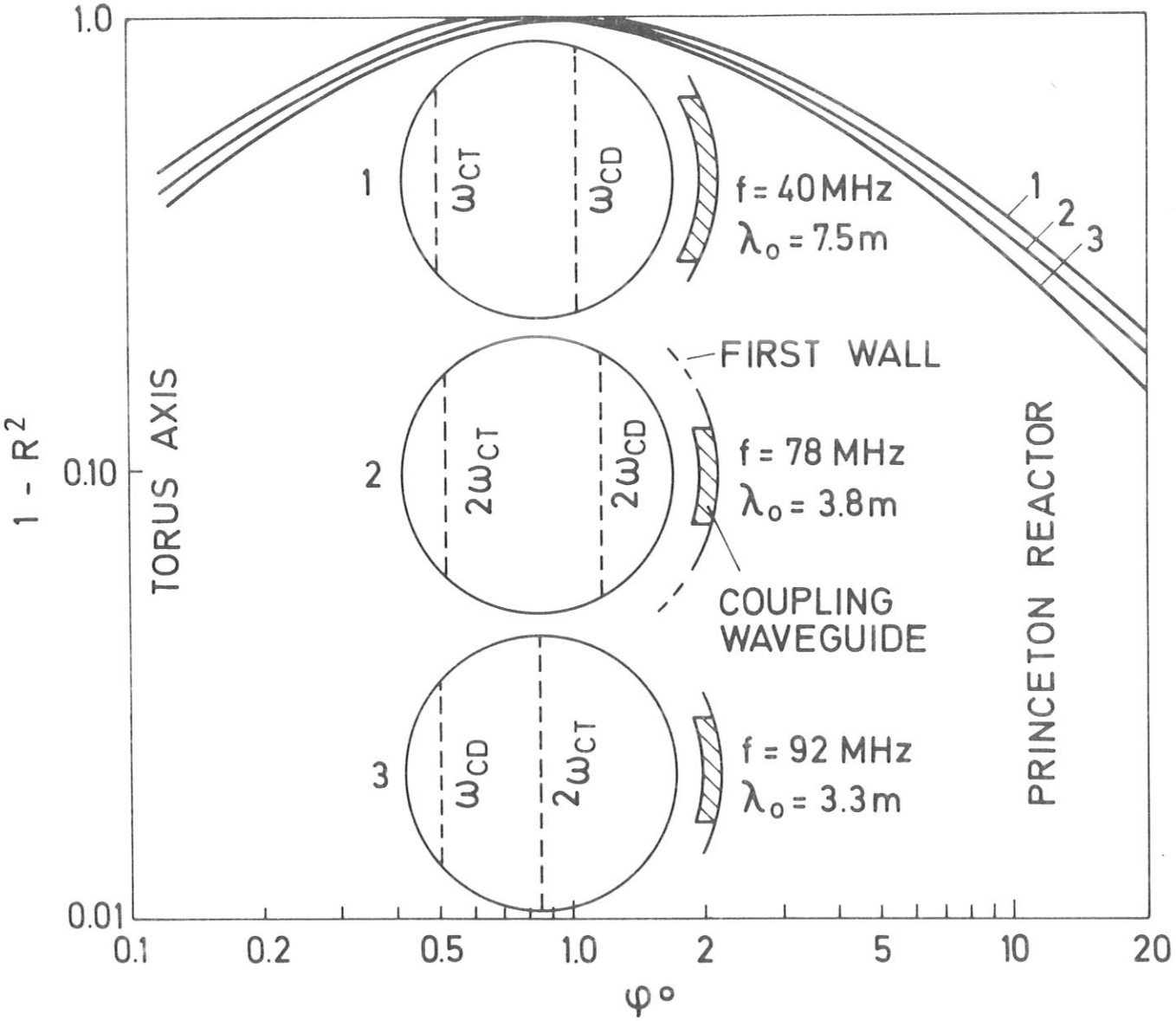
1.0
0.10
0.01
1 - R²
TORUS AXIS
PRINCETON REACTOR
1
2
3
ω_CT
ω_CD
2ω_CT
2ω_CD
f = 40 MHz
λ_o = 7.5m
f = 78 MHz
λ_o = 3.8m
f = 92 MHz
λ_o = 3.3m
FIRST WALL
COUPLING
WAVEGUIDE
0.1
0.2
0.5
1.0
2
5
10
20
φ°

Fig. 23

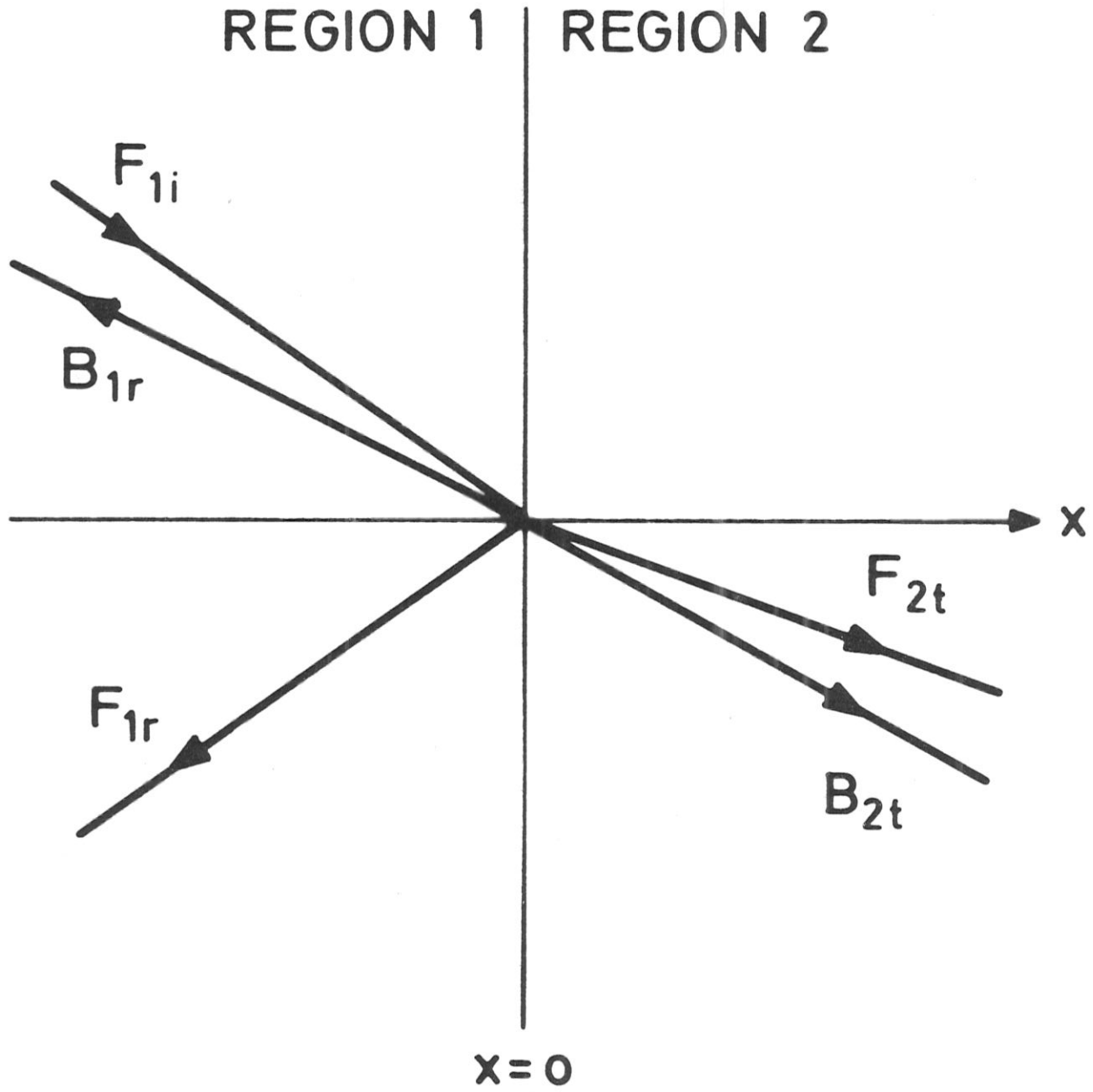

Fig. 24